**TECHNISCHE
UNIVERSITÄT
DRESDEN**

Introduction of a method for simulation of the proton therapy gantry at the Oncoray Dresden based on the Monte-Carlo-Tool TOPAS

Bachelor-Arbeit
zur Erlangung des Hochschulgrades
Bachelor of Science
im Bachelor-Studiengang Physik

vorgelegt von

Jan Eulitz
geboren am 11.4.1990 in Dresden

Institut für Kern- und Teilchenphysik
Fachrichtung Physik
Fakultät Mathematik und Naturwissenschaften
Technische Universität Dresden
2014

Eingereicht am 20. Oktober 2014

1. Gutachter: Prof. Dr. Arno Strassner
2. Gutachter: Prof. Dr. Wolfgang Enghardt

Abstract

Background and Purpose In medical physics there is a request of less complex, reliable and still flexible Monte Carlo software to simulate precisely experimental settings. This thesis will evaluate a new software named TOPAS (TOol for PArticle Simulation) [7] for proton therapy at Oncoray. TOPAS is developed at Massachusetts General Hospital and is currently in the beta-test phase. The evaluation is done in five steps: Firstly, simulated proton beam ranges R_0 are compared with NIST (National Institute of Standards and Technology) data [9] and lateral proton beam profiles are studied. Secondly, TOPAS results for multiple Coulomb scattering are collated with theoretic predictions from Highland's formula. Thirdly, an eye treatment beam line named Clatterbridge is reconstructed and analyzed in TOPAS. Fourthly, an own scattering setup is constructed, which enlarges the proton beam for cell irradiation experiments at Oncoray. Finally, the IBA (Ion Beam Applications) gantry in scanning mode is reconstructed using construction data provided by the IBA company and adjusted for Oncoray using experimental data from the commissioning measurements at Oncoray.

Materials and Methods TOPAS is used for constructions, simulations and visualizations of beam currents and beam lines. PYTHON is used for the analysis and visualization of 1D curves, 2D distributions and the polar plots.

Results The compiled results of this thesis are: Firstly, in the energy interval of [20|225] MeV the range difference between TOPAS and NIST are: $\Delta R_0 \leq 0.7$ mm. Secondly, for a single scattering foil of the thickness d_0 the multiple Coulomb scattering angle differences are: $\Delta\Theta_0 \leq 2$ mrad (lead, $d_0 = 0.1$ cm, beam energies $E \in [100|200]$ MeV). Fixing $E = 160$ MeV, the resulting differences are: $\Delta\Theta_0 \leq 3.3$ mrad (lead, $d_0 \in [0.02|1.0]$ cm); $\Delta\Theta_0 \leq 3.61$ mrad (copper, $d_0 \in [0.02|1.0]$ cm); $\Delta\Theta_0 \leq 3.04$ mrad (aluminum, $d_0 \in [0.06|1.0]$ cm); $\Delta\Theta_0 \leq 3.68$ mrad (lexan, $d_0 \in [0.1|6.0]$ cm). Thirdly, the Clatterbridge depth-dose-curve simulations lead to relative doses of: $D_{rel} \in [90|100]$ % in [0|2.5] cm depths and $D_{rel} \in [0|100]$ % in [2.5|3.0] cm depths. The lateral dose profile has a flat plateau spreading over 2.5 cm and a fall-off spreading over 0.5 cm. There is a relative proton fluence loss of approximately 1100 % and a relative neutron fluence loss of 47.35 %. Fourthly, the setup for cell irradiation experiments leads to a homogenous lateral dose profile with a flat plateau spreading over approximately 10.0 cm and a fall-off spreading over 1.0 cm. Finally, the range differences of TOPAS and the commissioning measurements of the IBA gantry in scanning mode are: $\Delta R_{0.9}$, $\Delta R_{0.8} \leq 1$ mm for the energies $E \in [140|226.7]$ MeV of the beam leaving the gantry. $\Delta R_{0.2} \approx 0.6$ mm at 140 MeV and increases linearly with around 0.03 mm/MeV. Fixing E and varying the beam energy spread σ for E=140 MeV and E=200 MeV the range differences are: $\Delta R_{0.9}$, $\Delta R_{0.8}$, $\Delta R_{0.2} \leq 0.6$ mm (E=140 MeV, σ=0.6 %) and $\Delta R_{0.9}$, $\Delta R_{0.8}$, $\Delta R_{0.2} \leq 0.5$ mm (E=140 MeV, σ=0.4 %).

Conclusions The following conclusions can be drawn: Firstly, TOPAS default settings deliver reliable results for proton beam ranges according to PSTAR for energies used in proton therapy. Secondly, for single scattering using Pb, Cu, Al and lexan scatter foils, TOPAS multiple Coulomb scattering angles differ from Highland's formula and the experimental data from [2], especially for scatter thicknesses $d_0 \leq 1$ mm. Other TOPAS physics lists should be tested to increase TOPAS multiple Coulomb scattering accuracy. Thirdly, the lateral dose profile and the depth-dose-curve of the Clatterbridge simulations satisfy the requirements of eye treatment radiation therapy. For the usage at Oncoray the beam energy could either be limited to the Clatterbridge energy of 62.2 MeV (f.e. by implementing material in front the beam line) or by optimizing the Clatterbridge construction to higher beam energies using the provided TOPAS files. Fourthly, a radiobiological experiment can be started, using the setup constructed for cell irradiation experiments. Finally, the TOPAS IBA gantry in scanning mode is adjusted using the commissioning measurements. In first approximation the TOPAS range R_{TOPAS} has to be decreased by 0.6 mm and the default beam energy spread σ has to be changed to 0.5 %. To increase the adjustments accuracy the optimized functions $E_0(E)$ and $\sigma(E)$ have to be calculated. E_0 is the energy corresponding to R_{TOPAS} and E the one corresponding to $R_{Measurement}$. The optimized energy shifts $\Delta E = E_0 - E$ MeV and σ has to be determined for every pair of Bragg peaks.

Zusammenfassung

Hintergrund und Ziele   In der medizinischen Physik gibt es einen Bedarf an übersichtlicher, vertrauenswürdiger und dabei immer noch flexibler Monte Carlo Software, für die präzise Simulation von Experimenten. Diese Arbeit evaluiert eine neue Software namens TOPAS [7] (TOol for PArticle Simulation) für die Protonenthearpie am Oncoray. TOPAS wird am Massachusetts General Hospital entwickelt und befindet sich derzeit in der Beta Testphase. Die Evaluation erfolgt in fünf Schritten: Erstens werden simulierte Protonenstrahlentiefen R_0 mit Daten aus NIST (National Institute of Standards and Technology) [9] verglichen und laterale Strahlenprofile untersucht. Zweitens werden Resultate von TOPAS für die Vielfach-Couloub-Streuung mit theoretischen Vorhersagen der Highlandformel verglichen. Drittens wird eine Anlage für Augenbestrahlungen, namens Clatterbridge, nachgebaut und analysiert. Viertens wird ein eigener Aufbau konstruiert, der den Protonenstrahl derart aufweitet, dass er für Zellbestrahlungsexperimente am Oncoray genutzt werden kann. Zuletzt wird die IBA (Ion Beam Applications) Anlage im Scannmodus nachgebaut, wofür Konstruktionsdaten des IBA Konzerns verwendet werden, und adjustiert unter Nutzung der experimentellen Daten aus den Messungen zur Inbetriebnahme der Anlage.

Materialien und Methoden   Die Monte Carlo Software TOPAS wird für Konstruktionen, Simulationen und Visualisierungen der Strahlen und Anlagen benutzt. PYTHON wird für die Analyse und Visualisierung der 1D Kurven, 2D Verteilungen und der Graphiken in Polarkoordinaten- Darstellung genutzt.

Ergebnisse   Die zusammengestellten Ergebnisse der Bachelorarbeit sind: Erstens gilt für die Strahlentiefendifferenzen zwischen TOPAS und NIST im Energiebereich von [20|225] MeV: $\Delta R_0 \leq 0{,}7$ mm. Zweitens ergeben sich für die Einfachstreuungen an Folien der Dicke d_0 die folgenden Winkeldifferenzen für die Vielfach-Coulomb-Streuung: $\Delta \Theta_0 \leq 2$ mrad (Blei, $d_0 = 0{,}1$ cm, Strahlenenergien $E \in [100|200]$ MeV). Legt man E auf 160 MeV fest, dann sind die resultierenden Differenzen: $\Delta \Theta_0 \leq 3{,}3$ mrad (Blei, $d_0 \in [0{,}02|1{,}0]$ cm); $\Delta \Theta_0 \leq 3{,}61$ mrad (Kupfer, $d_0 \in [0{,}02|1{,}0]$ cm); $\Delta \Theta_0 \leq 3{,}04$ mrad (Aluminium, $d_0 \in [0{,}06|1{,}0]$ cm); $\Delta \Theta_0 \leq 3{,}68$ mrad (Lexan, $d_0 \in [0{,}1|6{,}0]$ cm). Drittens führt die Simulation von Tiefendosiskurven der Clatterbridge Anlage zu den relativen Dosen: $D_{rel} \in [90|100]$ % in Tiefen von $[0|2{,}5]$ cm und $D_{rel} \in [0|100]$ % in Tifen von $[2{,}5|3{,}0]$ cm. Das laterale Dosisprofil besteht aus einem flachen Plateau von 2,5 cm Breite und einem 0,5 cm breiten Abfallbereich. Es gibt eine relativen Protonenfluenz- Verlust von ca. 1100 % und einen relativen Neutronenfluenz- Verlust von 47,35 %. Viertens führt die Simulation des Aufbaus für die Zellbestrahlungsexperimente zu einem homogenen lateralen Dosisprofil mit einem flachen, ca. 10 cm breiten Plateau und einem ca. 1 cm breiten Abfallbereich. Zuletzt ergeben sich die folgenden Strahlentiefendifferenzen zwischen TOPAS und den experimentellen Messungen zur Inbetriebnahme an der IBA Anlage

im Scannmodus von: $\Delta R_{0,9}$, $\Delta R_{0,8} \leq 1$ mm für die Energien E $\in$ [140|226,7] MeV des Strahls der die Anlage verlässt. $\Delta R_{0,2} \approx 0,6$ mm bei 140 MeV und nimmt linear zu mit ca. 0,03 mm/MeV. Setzt man E fest und variiert die Breite des Energiespektrums des Strahls σ, dann ergeben sich für E=140 MeV und E=200 MeV die folgenden Strahltiefendifferenzen: $\Delta R_{0,9}$, $\Delta R_{0,8}$, $\Delta R_{0,2} \leq 0,6$ mm (E=140 MeV, σ=0,6 %) und $\Delta R_{0,9}$, $\Delta R_{0,8}$, $\Delta R_{0,2} \leq 0,5$ mm (E=140 MeV, σ=0,4 %).

Schlussfolgerungen Die folgenden Schlussfolgerungen können gezogen werden: Erstens liefern die TOPAS Standardeinstellungen, nach PSTAR, zuverlässige Ergebnisse für Strahltiefen von Protonenstrahlen in einem klinisch relevanten Bereich. Zweitens unterscheiden sich, für die Einfachstreuungan an Pb, Cu, Al und Lexan Folien, die in TOPAS simulierten Vielfach-Coulomb-Streuungswinkel von der Highlandformel und den experimentellen Daten aus [2], besonders für Folienbreiten $d_0 \leq 1$ mm. Um die Genauigkeit von TOPAS für die Vielfach-Coulomb-Streuung zu verbessern sollten andere TOPAS Physiklisten getestet werden. Drittens führt die Simulation der Clatterbridge Anlage zu zu lateralen Dosisverteilungen und Tiefendosiskurven, die den Anforderungen für Augenbehandlungen in der Strahlentherapie gerecht werden. Für die Benutzung der Anlage am Oncoray kann der Strahl entweder auf die Clatterbridge Strahlenenergie von 62,2 MeV gebremst werden durch Materialien, die vor der Anlage implementiert werden, oder der Clatterbridge Aufbau wird unter Nutzung der bereit gestellten TOPAS Dateien für höhere Energien optimiert. Viertens kann auf der Grundlage des Aufbaus für die Zellbestrahlungen ein Radiobiologieexperiment durchgeführt werden. Zuletzt wird die TOPAS IBA Anlage im Scannmodus mit Hilfe der Messungen zur Inbetriebnahme adjustiert. In erster Näherung muss die TOPAS Strahlentiefe R_{TOPAS} um 0,6 mm verringert werden und die Standardeinstellung der Breite des Energiespektrums auf 0,5 % geändert werden. Um die Genauigkeit der Adjustierung zu verbessern müssen die Optimierungsfunktionen $E_0(E)$ and $\sigma(E)$ berechnet werden. E_0 ist die Energie zur Strahlentiefe R_{TOPAS} gehört und E die Energie zur Strahlentiefe $R_{Measurement}$. Die optimierten Energieänderungen $\Delta E = E_0 - E$ MeV und σ müssen dabei für jedes Paar von Tiefendosiskurven bestimmt werden.

Schlüsselwörter TOPAS, Monte Carlo, NIST, Bragg peak, spread out Bragg peak, range modulation wheel, Vielfach-Coulomb-Streuung, Highland's Formel, Clatterbridge, IBA

Contents

1 Introduction

Cancer is among the leading causes of death worldwide, accounting with 8,2 Million deaths in 2012 [1]. The most common cancer deaths are lung (1.59 million deaths), liver (745,000 deaths), colorectal (694,000 deaths), breast (521,000 deaths) and oesophageal cancer (400,000 deaths). In Germany in 2012 every 4th death was caused by cancer [1]. Next to resection (operative excision of the tumor) and medicamental treatments (chemotherapy, immuntherapy,...) radiation therapy is a main cancer treatment method. Radioactive substances, X-rays (Roentgen radiation), electrons, neutrons, protons and heavier ions destroy cancer cells through electromagnetic and nuclear interactions. The main advantage of ion therapy, compared to X-rays, is the reduction of total energy deposited in the patient and the finite range. Compared to heavier ions, protons deposit less energy in the target, but are easier to produce and clinically more comparable to X-rays. Proton therapy is in present the cheapest and most spread ion therapy.
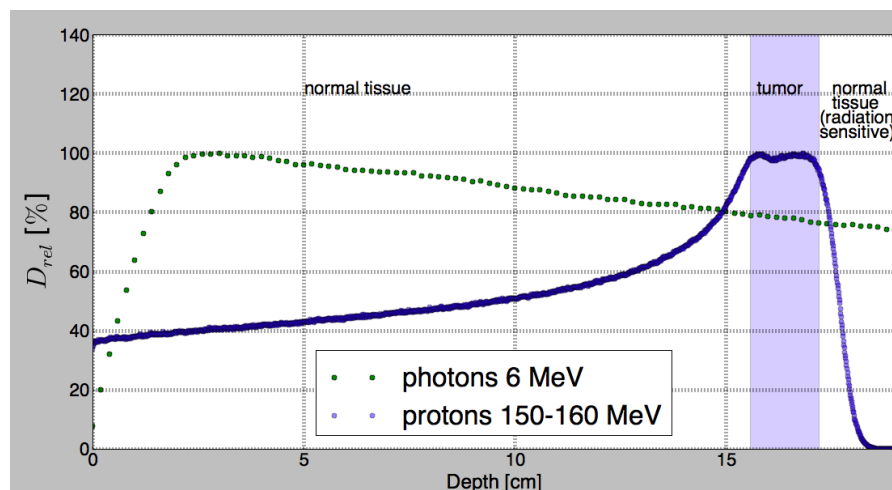
Figure 1.1: Comparison of photon and proton depth-dose-curves. A monoenergetic photon beam of 6 MeV with circular shape (radius=0.5 cm) hits a water target as shown in Figure 4.1. The spread out Bragg peak proton beam is constructed by protons in ranges between 150-160 MeV.

Monte Carlo simulations are significantly important in radiation therapy, because the patient cannot be used for experiments. Monte Carlo codes simulate precisely experimental conditions and save beam time. They can be used for a prediction of the delivered dose distribution to the patient, for studying proton beam physics, for designing the treatment head and quality ensurance [11, chapter 9]. The available general purpose Monte Carlo software on the market

have been overly complex for the most clinical medical physics. This bachelor thesis studies a new Monte Carlo software named TOPAS and shows its performance in constructing, simulating and scoring of clinical settings.

The proton therapy gantry at Oncoray includes a clinical beam line and a beam, which can be used for experiments. Both are ready to use now leading to the necessity of characterizing the clinical beam line and to design an experimental beam line, which can be used for radiobiology experiments. This bachelor thesis uses TOPAS to simulate the clinical beam line and to design an experimental one. There are four basic goals:

(I) providing a helpful addition in learning the TOPAS program language

(II) checking the accuracy of the TOPAS default parameters in reproducing basic physical interactions, correct proton beam ranges, lateral beam profiles and multiple Coulomb scattering angles

(III) giving a prediction of optimal parameters of a setup for cell irradiation experiments

(IV) adjusting the IBA scanning nozzle in TOPAS to the commissioning measurements

These goals are tried to achieve in 7 chapters. Before starting to simulate Oncoray settings a theory chapter will provide a short overview over proton therapy physics and the following chapters test TOPAS default parameters.

The theory chapter 2 introduces basic proton interactions in matter for proton therapy and discusses range modulation and scattering techniques used in proton therapy. A macroscopical and mathematical description of a proton beam and the functional principle of Monte Carlo codes are briefly introduced. A discussion of the Geant4 and the TOPAS software end up the chapter. The chapter gives a short overview over proton therapy physics from a physical point of view and over the software that is used in this thesis.

Chapter 3 introduces basic TOPAS geometries and special components. Detailed software information are discussed in the appendix in chapter A. In section B.1 a TOPAS example file is provided which can be used for the simulation of Bragg peaks. Beam currents of protons, electrons, neutrons, photons and alpha particles are studied and the observed physical interactions are discussed. This chapter aims to support visually the apprehension of TOPAS functionality and to check visually if expected beam physics is reproduced.

In Chapter 4 1D depth-dose-curves and 2D depth-dose-distributions of protons in water are simulated and studied. The proton ranges R_0 are determined and compared with NIST data. Lateral proton beam distributions are studied and are set in contrast to lateral beam distributions of alpha particles and photons. The construction of spread out Bragg peaks using TOPAS time mode is introduced. This chapter tests TOPAS in reproducing correct proton beam ranges and lateral profiles.

Different scattering systems are studied in Chapter 5. Scattering angles of proton beams are simulated and compared with predictions from Highland's formula. An eye cancer treatment beam line named Clatterbridge is constructed, simulated and analyzed. For cell irradiation experiments at Oncoray a setup is constructed and studied. The chapter tests the multiple Coulomb scattering physics of the TOPAS default settings and its functionality in constructing and simulating settings of higher complexity compared to the previous chapters.

Chapter 6 simulates the IBA gantry in scanning mode based on the construction data from the IBA company. Simulated proton ranges are compared with measurements from the commissioning. Range differences are analyzed for different beam energies and beam energy spreads. This chapter shows the accuracy of TOPAS in simulating the IBA scanning nozzle.

The conclusion chapter 7 summarizes the observed results, discusses accuracy and errors and points out problems and tasks which can be resumed on base of this thesis. The range differences of TOPAS data to PSTAR are estimated and the error calculation for the range analysis and for Monte Carlo codes in general are discussed. The lateral beam profiles are explained by the underlying physics interactions. For the TOPAS spread out Bragg peak construction the relevance of an optimization algorithm is described. For multiple Coulomb scattering in TOPAS possible error sources are listed and validated. The observed scorings of the scattering systems and the IBA gantry are explained and the impacts for experiments at Oncoray are discussed.

2 Theory of Proton Interactions in Matter

This chapter provides an overview over the basic proton interactions in matter for proton therapy. By describing stopping and scattering the techniques will be introduced, that are used for range modulation and scattering in proton therapy. The discussion of the proton interactions will end up in a complete explanation of the full Bragg peak shape. A macroscopical and mathematical description of the proton beam in matter follows. The functional principle of Monte Carlo codes and how Monte Carlo simulations are used in proton therapy are briefly introduced.

For proton therapy there are three important interactions of protons in matter: stopping, scattering and nuclear interactions, whereby stopping and scattering are dominated by electromagnetic interactions between protons and electrons and the nuclear interactions happen through the strong interaction between protons and neutrons.

2.1 Stopping

The main stopping effect of the protons are collisions with atomic electrons. The stopping power increases when a proton slows down, because of the longer electromagnetic interaction time.

Bethe Bloch Equation

The curve of stopping power as a function of kinetic energy is described by the Bethe-Bloch-equation which can be derived through Rutherford-scattering, relativistic energy-impuls-relations and through an integral over oscillator strengths between all states.

$$-\frac{dE}{dx} = \underbrace{4\pi N_A r_e^2 m_e c^2}_{(i)} \cdot \underbrace{z}_{ii} \cdot \underbrace{\frac{Z}{A}}_{(iii)} \cdot \underbrace{\rho}_{(iv)} \cdot \underbrace{\frac{1}{\beta^2}}_{(v)} \cdot \underbrace{\left(\ln \frac{W_m}{I} - \beta^2 + corrections \right)}_{(vi)} \qquad (2.1)$$

$$W_m = \frac{2m_e \cdot c^2 \cdot \beta^2}{1 - \beta^2} \qquad \beta = \frac{v}{c} \qquad m_e c^2 \approx 0,511 \text{MeV} \qquad (2.2)$$

(i) is a material-independent constant of approximately 0.3072. (ii) is the atomic number of the entering particles (z=1 for protons). (iii) is the amount of electrons in matter which is approximately 0.5 for light atoms. (iv) is the mass density of target matter. Multiplied with Avogardonumber N_A and divided with the atomic mass it can be transformed into particle density which is a characteristic value for energy loss in a infinitesimal path length. (v) characterizes the inverse velocity of the particles and (vi) the probability of an energy transfer from a proton to an electron. W_m is the largest possible energy loss in a single collision with a free electron and I the mean excitation energy. In a radiotherapy energy regime $(3 - 300$ MeV) it is permissible to neglect any correction terms which leads to a mass stopping power for protons in matter of [11, p. 33]:

$$\frac{S_{el}}{\rho} \equiv -\frac{1}{\rho} \cdot \frac{dE}{dx} = 0,3072\frac{Z}{A}\frac{1}{\beta^2}\left(\ln\frac{W_m}{I} - \beta^2\right)\frac{\text{MeV}}{\text{g/cm}^2} \tag{2.3}$$

The mean excitation energy of an atomic electron of the target material I cannot be calculated from first principles. It is roughly proportionate to Z $(I/Z \approx 10eV)$, but interpolation is difficult because of irregularities in the atomic shell structure. For example water in TOPAS has a mean excitation energy of 75 eV, which is the value used in commissioning tests at Massachusetts General Hospital and differs from Geant4-water value of 78 eV defined in NIST. In TOPAS it is possible to use both water types [12, p. 20]. If the target material consists out of a mixture of elements Bragg's additivity rule can be used, which is just a good approximation if the mixture can be approximated as a succession of very thin sheets of the different non interacting atoms.

$$\frac{S}{\rho} = \sum_i w_i \left(\frac{S}{\rho}\right)_i \qquad w_i... \text{ fraction by weight} \tag{2.4}$$

Mean Projected Range

The mean projected range (or just range) of a proton beam R_0 is defined as the depth of material at which half of the protons have stopped by undergoing just electromagnetic interactions. It corresponds to the dose of 80% of maximum dose after the Bragg peak for a proton beam in water. The mean projected range is approximately the total path length R, just a little bit smaller $(R_{total} = 0,998 \cdot R_0$ for 100 MeV protons in water [11, p. 35]).

$$R_0 \approx R_{total}(E_{initial}) = \int_{E_{initial}}^{E_{final}} \left(\frac{1}{\rho}\frac{dE}{dx}\right)^{-1} dE = \int_{E_{initial}}^{E_{final}} \frac{dE}{S/\rho} \tag{2.5}$$

In light atom targets nucleus density is small and multiple Coulomb scattering effects are

negligible. Scattering through electron collisions has a small effect too, because protons are much heavier than electrons. So mean projected range can be calculated numerically. With $\frac{S}{\rho}$ as a function of β, and so E, the mean projected range for a proton entering the target with $E_{initial}$, and stopping at a small value E_{final} can be calculated by using the continuous slowing down approximation [11, p. 34]:

Range Modulation Techniques

A Bragg peak is too narrow to cover a target volume in proton therapy. Therefore, combinations of proton beams of decreasing energy are used to modulate the range to obtain a uniform depth-dose-region called spread out Bragg peak(SOBP). The shifted in depth Bragg peaks are weighted and summed to the SOBP depending on the target size:

$$SOBP() = \sum_{i=1}^{N} w_i \cdot PP(R_i, d) \tag{2.6}$$

$PP(R_i, d)$ is the pristine peak depth-dose curve with Range R_i and w_i the relative contribution of peak i. In proton therapy different techniques are used to produce SOBP: energy stacking, range modulation wheels and ridge filters. Energy stacking means changing directly the energy of protons entering the gantry on an accelerator level. The advantage is the non interacting of protons with range shifters inside the nozzle. One big disadvantage is, that not only the accelerator energy has to be changed, also the transport magnets need to be adjusted, which is technological complicated, and so this technique is not as spread as the range modulation wheels in proton therapy [11, p. 133]. Range modulation wheels consist out of steps of varying thickness, whereby each step corresponds to a pristine peak in the spread out Bragg peak. They are made of low-Z materials to limit scattering (plastic, lexan,...). For wheels that need to provide large range shifts in nozzles where space is limited also carbon and aluminum have been applied [11, p. 134]. The principle of ridge filters is the same as for range modulation wheels. The thickness of the ridge filter steps determines the pullback of the peaks, and the width of the steps sets the weight of the peaks [11, p. 140].
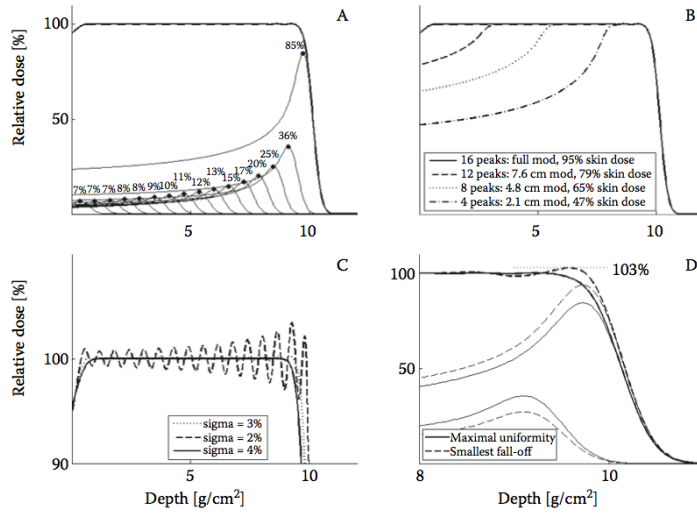
Figure 2.1: Creation of a spread out Bragg peak with a range of $10g/cm^3$. A: weights of the pristine peaks, B: various modulation width, C: effect of change in the pristine peak on the spread out Bragg peak without re-optimization, D: alternative methods of optimization at the distal fall-off of the spread out Bragg peak [11, p. 131].
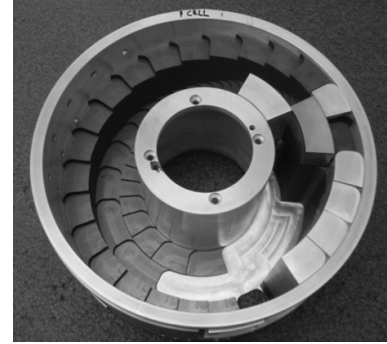
Figure 2.2: IBA range modulation wheel. The range modulation wheel from combines three range modulation tracks [11, p. 135].
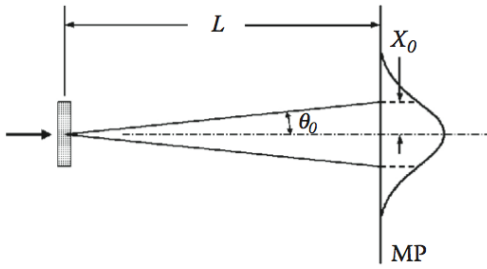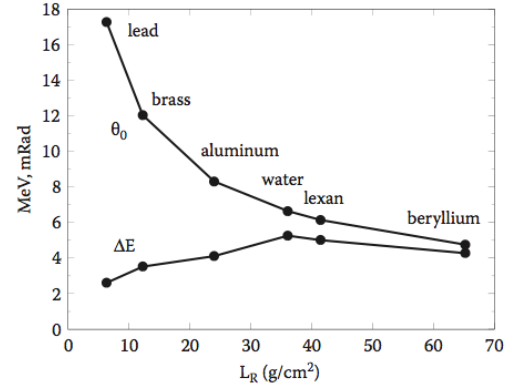
2.2 Scattering

Multi Coulomb Scattering

Scattering of protons in matter happens through many electromagnetic collisions with atomic nuclei and is called multiple Coulomb scattering . The main effect for the angular distribution is statistically (random walk in angle [11, p. 37]), because the angular deflection of a single scattering event is almost negligible. The sum of all small random deflections leads to an angular distribution with a Gaussian core and a single scattering tail from the not quite rare large single scatterers in the target. For clinical approach usually just the Gaussian part has to be considered for multiple Coulomb scattering , which contains about 98% of the protons [11, p. 37]). Figure 2.3 shows an ideal proton beam entering a target, drifting through the distance L, and with no additional scattering at the measurement plane MP leading to a root mean square (rms) spread of X_0. Fluence can be measured with a dosimeter, because all protons entering the measuring plane have nearly the same energy or stopping power and so dose is proportional to fluence. There are a lot of measured values of Θ_0 for a large assortment of thicknesses and target materials [11, p. 38] [2].

$$\Theta_0 \approx \tan \Theta_0 = \frac{X_0}{L} \qquad \xrightarrow{L >> X_0} \qquad X_0 \approx L \cdot \Theta_0 \qquad\qquad (2.7)$$

Figure 2.3: Multiple Coulomb scattering Setting. Multiple Coulomb scattering in a thin slap, MP: measuring plane, X_0: root mean square spread, Θ_0: usually smaller than 16° [11, p. 23].

Figure 2.4: Multiple Coulomb scattering angle and energy loss. Multiple scattering angle and energy loss for 160-MeV protons traversing 1 g/cm2 of various materials, data from [9] [11, p. 23]

Highland's Formula and Molière's Theory

In Gaussian approximation the dependence of Θ_0 on scattering material and proton energy is described by Highland's formula.

$$\Theta_0 = \frac{14.1\text{MeV}}{pv}\sqrt{\frac{D_S}{L_R}}\left[1 + \frac{1}{9}log_{10}\left(\frac{D_S}{L_R}\right)\right]\text{ rad} \tag{2.8}$$

$$D_S = d_S \cdot \rho_S \qquad d_S \text{ ... scatter thickness} \quad \rho_S \text{ ... scatter material density} \tag{2.9}$$

$$\tau \equiv \frac{E}{mc^2}\text{... reduced kinetic energy} \tag{2.10}$$

$$pv = \frac{\tau+2}{\tau+1}E = 297\text{MeV}(E = 160\text{MeV}) \tag{2.11}$$

$$L_R = \frac{1432.8 \cdot A}{Z(Z+1)(11.319 - \ln Z)}\frac{\text{g}}{\text{cm}^2} \text{ ... radiation length of the scatter material} \tag{2.12}$$

14.1 MeV is a numerical constant [11], pv the kinematic factor, d_S the scatter thickness and L_R the radiation length of the scatter material, which can be found in tables. Highland derived his formula by fitting a version of Molières's theory, which is algebraically complicated, but important for proton radiotherapy, because of generalizations to scattering in arbitrarily thick targets (large proton energy loss) and compounds of mixtures [11, p. 38]. The simplest case of Molières's theory (sufficiently thin target of one element) is discussed in [11, p. 39-43]. Molière approximated the angular distribution as a power series in $1/B$, where B is the reduced target thickness. The first summand is Gaussian. Figure 2.5 shows, that the Gaussian summand fits

the experimental data much worse compared to the complete Molierè power series. Highland parameterized the full Molière's theory, with additions from Bethe and Hanson, in a satisfying way, which fits most experimental data (Figure 2.6).
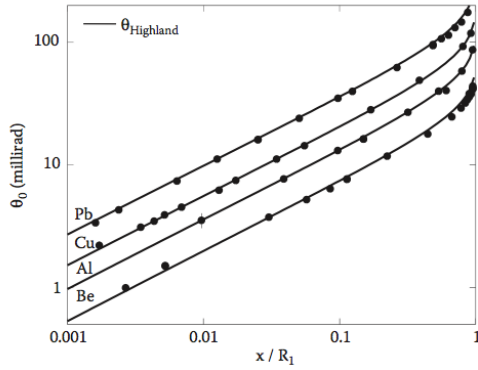
Figure 2.5: Accuracy of Highland's formula for four elements. x/R_1 is target thickness divided by proton range at the inicident energy. The points are experimental data at 158.6 MeV from [2].
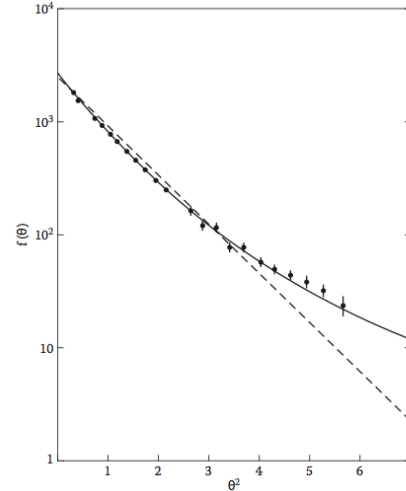
Figure 2.6: Comparison of Gaussian Approximation (straight line), Molière's theory (solid line) and experimental data from Hans Bichsel [3].

Scattering Techniques

The easiest way to construct a scattering system is a flat scatterer, that spreads the beam in a Gaussian like profile (Figure 2.7). A collimator (aperture) blocks the beam outside a central high dose region. Because of the relative sharp shape of a Gaussian profile single scatterer have a low efficiency and are limited to small fields not exceeding $\approx 7cm$. The efficiency η is defined by the proportion of protons inside a useful radius:

$$\eta = 1 - e^{-\frac{1}{2}(R/\sigma)^2} \qquad \sigma... \text{ Gaussian spread} \qquad R... \text{ useful radius} \qquad (2.13)$$

The fraction of protons outside the useful radius is equal to the relative dose at the useful radius when normalizing to central axis. When we allow a dose variation of $\pm 2, 5\%$ over the profile and setting the useful radius to 95%, this leads to an efficiency of only $\eta = 100\% - 95\% = 5\%$. Because of the field size limitation and the sharp dose falloff, single scattering is ideal for eye treatments [11, p. 126].

Figure 2.8: IBA contoured scatterer. Shematic cross section of an energy-compensated contoured scatterer in the IBA universal nozzle [11, p. 129].
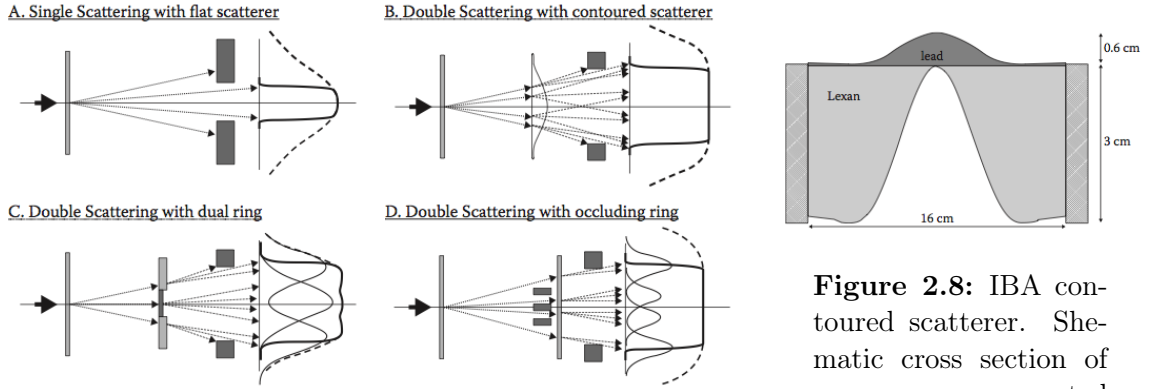
Figure 2.7: Scattering systems. A: single flat scatterer, B: double scattering with contoured scatterer, C: dual ring double scattering, D: occluding ring double scattering [11, p. 127].

A flatter profile and better efficiencies can be achieved by scattering more of the central protons outside by using a second scatterer, which can be a contoured scatterer, a dual ring or a second flat scatterer combined with occluding rings (Figure 2.7). A contoured scatter is an optimized combination consisting out of a high and a low scattering material as you can see in figure 2.8. The mathematical dose distribution $\Phi(r)$ of a double-scattering system can be described as follows:

$$\Phi(r) = \frac{1}{(2\pi z_{FS}\Theta_{FS})} \int_0^{2\pi} d\Phi \int_0^R \vec{r'}d\vec{r'} \cdot \underbrace{\exp\left[-\frac{\vec{r'}^2}{(z_{FS}\Theta_{FS})^2}\right]}_{(i)} \cdot \frac{1}{(z_{CS}\Theta_{CS}(\vec{r'}))^2} \tag{2.14}$$

$$\cdot \underbrace{\exp\left[-\frac{(\vec{r}-\vec{r'})^2}{(z_{CS}\Theta_{CS}(\vec{r'}))^2}\right]}_{(ii)} \tag{2.15}$$

z_{FS} and z_{CS} are the distance from the first and second scatterer to the plane of interest, Θ_{FS} is the characteristic angle of the first flat scatterer, which is constant, Θ_{CS} is the characteristic scattering angle of the contoured scatterer, that depends on radial position $\vec{r'}$. R is the radius of the contoured scatterer assuming all protons outside R are blocked. The radial coordinates $\vec{r'}$ and R of the contoured scatterer are projected from the first scatterer onto the plane of interest. The first exponential term (i) describes the fluence of the beam hitting the contoured scatterer at position $\vec{r'}$. The second exponential term (ii) describes the contoured scatterer, which means the proportion of protons hitting the second scatterer at position $\vec{r'}$ and ending up at position $\vec{r}$. This depends on the distance between $\vec{r'}$ and $\vec{r}$ and the angular spread of

the contoured scatterer. Simplifications in this formula are: Gaussian scattering, rotational symmetry, thin scatterers and a small parallel entrance beam [11, p. 128].

2.3 Nuclear Interactions

Nuclear interactions are rare and the electromagnetic interactions of protons dominate. They are harder to model than stopping and scattering and have a low biological effect. But they are still important because of production of free neutrons which can travel long distances without interacting and leaving dose in areas far away from the tumor target through collisions with protons.

Elastic, Inelastic, Nonelastic

There are three types of nuclear interaction: elastic, nonelastic and inelastic. In an elastic interaction total kinetic energy is conserved and target nuclei and projectile are unchanged by the reaction. In nonelastic and inelastic interactions total kinetic energy is not conserved. While in inelastic interactions final nucleus are the same as the bombarded nuclei in nonelastic reactions the target can undergo breakup or can be excited in higher quantum state. Also particle transfer reaction may occur [11, p. 46] [14]. So $^{16}O(p,p)^{16}O$ is an elastic reaction, $^{16}O(p,p)^{16}O^*$ (* means excited state) is inelastic and $^{16}O(p,2p)^{15}N$ is nonelastic. All protons from the source which slow down in the material are called primaries where particles from inelastic or nonelastic interactions called secondaries. Protons in H_2O can scatter with hydrogen at a relative angle of approximately 90°, share the original kinetic energy and may appear as secondaries. Therefore, they should be included in any counting of secondaries [11, p. 47].

Secondaries

Protons, neutrons, γ-rays, heavy fragments such as alphas and recoiling residual nuclei are possible secondaries from nonelastic interactions in a therapy energy regime, whereby heavier fragments than alphas are rare. Table 2.1 shows the fractions of $E_{initial}$ carried away for secondaries of a 150 MeV proton beam modeled by Monte Carlo simulations by Seltzer [14]. Heavy fragments carry little energy and that is why they have a lower relative biological effect (RBE), despite their high-ionization density [11, p. 48].

Particle	p	deuterium	tritium	^3He	α	Recoils	n
Fraction $E_{initial}$	0,57	0,016	0,002	0,002	0,029	0,016	0,20

Table 2.1: Fractions of energy carried away by secondaries for 150 MeV proton beam [11, p. 47].

Full Bragg Peak Description

These three interactions stopping, scattering and nuclear interactions are sufficient to explain the Bragg peak. Figure 2.9 shows and explains the different parts of the Bragg peak curve.
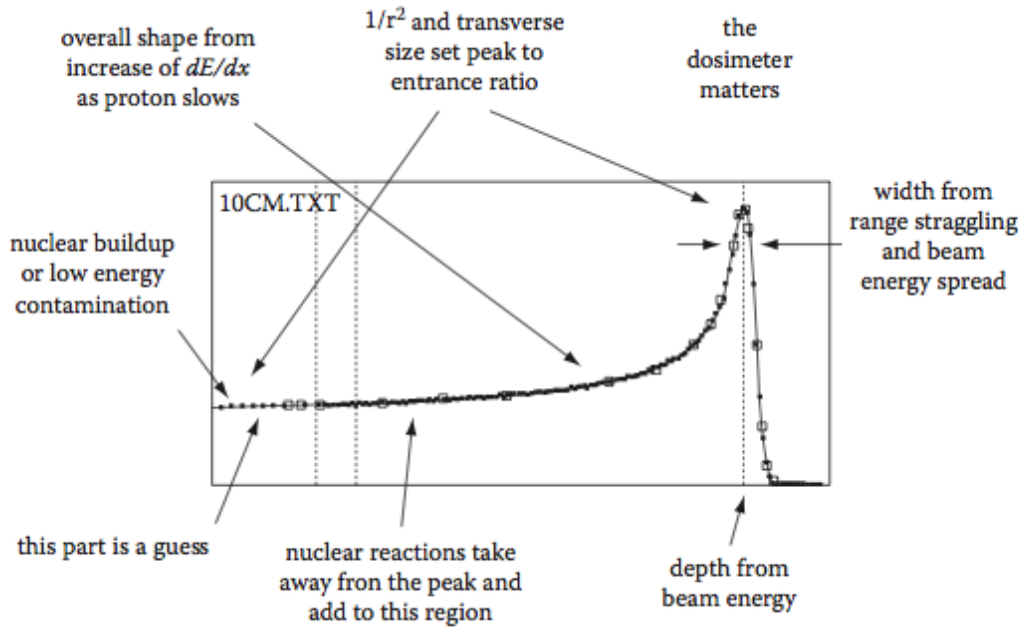
Figure 2.9: Explanation of Bragg peak curve. Explanation of the different parts of the Bragg peak curve [11, p. 52].

2.4 Macroscopic Beam Description

To describe a proton beam in matter it is useful to define the following physical values:

$$\Phi = \frac{dN}{dA} \frac{\text{protons}}{\text{cm}^2}...\text{fluence}, \qquad \dot{\Phi} = \frac{d\Phi}{dt} \frac{\text{protons}}{\text{cm}^2 \cdot \text{s}}...\text{fluence rate}, \tag{2.16}$$

$$S = -\frac{dE}{dx} \frac{\text{MeV}}{\text{cm}}...\text{stopping power} \tag{2.17}$$

$$\frac{S}{\rho} = -\frac{1}{\rho} \cdot \frac{dE}{dx} \frac{\text{Mev}}{\text{g/cm}^2}...\text{mass stopping power}, \tag{2.18}$$

$$D \equiv \frac{\text{energy}}{\text{mass}} = \frac{dE/dx \cdot dx \cdot dN}{\rho \cdot dA \cdot dx} = \Phi \cdot \frac{S}{\rho}...\text{dose} \tag{2.19}$$

$$\dot{D} = \dot{\Phi} \cdot \frac{S}{\rho} = \frac{e \cdot \dot{N}}{A} \cdot \frac{S}{\rho} = \frac{i_p}{A} \cdot \frac{S}{\rho} \frac{\text{Gy}}{\text{s}}...\text{dose rate} \tag{2.20}$$

$\frac{i_p}{A}$ is the current density. For protons with an energy of 170 MeV in water (S=5 MeV/(g/cm^2)) a typical radiotherapy dose rate is 0.017 Gy/s=1Gy/min which leads to a value of 0.0033nA/cm^2.

In a scattering system not all protons from the source reach the scorer, so it is useful to introduce a efficiency factor ϵ, which is for a single scatterer around 0.05 and a double scatterer around 0.45. The dose at the Bragg-Peak is around $f_{BP} = 3.5$ times higher (typical factor) than at the entrance of the target, so dose rate have to be multiplied with this factor. To create a SOBP the deepest step has to be irradiated the longest time (dwell time). To create a flat curve the other Bragg peaks are treated only a fraction of this dwell time, which is described with this factor f_{mod}. f_{mod} depends on the modulation and is ≤ 1. For zero modulation it is 1. This leads to a formula for an average dose rate over one modulation cycle of a Bragg peak in a scattering range modulated system:

$$< \dot{D} > = \epsilon \cdot f_{BP} \cdot f_{Mod} \cdot \frac{i_p}{A} \cdot \frac{S}{\rho} \frac{Gy}{s} \tag{2.21}$$

2.5 Boltzmann Transport Equation

Transport Equation

Mathematically the proton transport in matter can be accurately described with the steady state, linear Boltzmann Transport Equation, which is an integro-differential equation containing six independent variables and describing the angular flux $\phi(\vec{r}, E, \Omega)$ [15, p. 19]. The angular flux can be interpreted as the particle density with the kinetic energy E, moving in a direction Ω through the surface of the unit sphere at position $\vec{r}$.

$$\underbrace{\Omega \cdot \nabla \phi(\vec{r}, E, \Omega)}_{streaming\ term} + \underbrace{\sigma_t \cdot \phi(\vec{r}, E, \Omega)}_{total\ removal\ term} = \underbrace{\int_{4\pi} d\Omega' \int_0 dE' \sigma_s(\vec{r}, E' \to E, \Omega' \to \Omega) \cdot \phi(\vec{r}, E', \Omega')}_{Boltzmann\ operator}$$

$$\tag{2.22}$$

The streaming term describes the free movement of the particles through the matter. The total removal term describes all interactions of the particles, causing the particles to scatter to an energy different from E and a direction different from Ω. The Boltzmann operator describes particles scattered from all the energy E' and directions of movement Ω' [15, p. 19-20]. The operator can be separated in the different scattering types: non-elastic scattering, inelastic scattering with atomic electrons and elastic scattering with atomic nuclei [15, p. 21].

Assumptions

Four assumptions are made for using this equation [15, p. 19-20]:

(i) Free motion of particles can be described through classical mechanics.

(ii) There are only binary collisions, three body collisions are negligible, because the proton density is in the order of $10^{10}\ cm^{-3}$ and atom density of typical tissue is around $10^{23}\ cm^{-3}$.

(iii) No proton-proton interaction takes place, because number of free protons is much smaller compared to the number of atoms in tissue so that the proton charges are screened from each other through the atomic electrons.

(iv) The properties of the host medium are not altered, which can be justified with the small non-elastic cross sections.

Discussion and Solving The linear Boltzmann equation describes only the mean particle density distribution. Because interaction of protons in matter is a stochastic process there are fluctuations in the distribution, which can be captured by adding more terms in the equation. In most cases capturing fluctuations is not necessary, because the only interesting value is the total deposited energy, which can be obtained by integrating the average dose deposition over time [15, p. 21]. Solving Boltzmann equation can be done by transforming the equation in an integral form and solving this form either numerically stochastically with Monte Carlo integration methods, or numerically deterministically (e.g .with finit element method). The Monte Carlo algorithms have the advantage, that they are less sensitive to singularities and work selective in the target volume in the phase space.

2.6 Monte Carlo Simulations

Monte Carlo simulations uses algorithms to solve numerically problems which are hard or not analytically solvable, by using stochastic theorems.

Monte Carlo Algorithms

Monte Carlo codes are allowed to calculate a statistically fluctuating solution with a bounded up probability. With repetitions of the algorithm with independent random orbits the error probability can be decreased. A calculation of the irrational number π can be arranged by counting random numbers on a quadratic plane with a circle in it that way, every time the random point is in the circle it is counted separately.

$$\frac{\text{Circle Surface}}{\text{Square Surface}} = \frac{\pi r^2}{(2r)^2} = \frac{\pi}{4} = \frac{\text{Points in the Circle}}{\text{All generated Points}} \tag{2.23}$$

With this method areas under functions can be calculated and so numerical integration for any desired high dimensional integral. Usually the integrated area is too large and so a so called Markow-chain is used which is a chain of points with a distribution and spread over

the integration area that represents the integral. Depending on the physical problem it can be hard to find a suitable spread Mankow-chain, if the chain covers the whole integration area, the algorithm is ergodic. The mathematically background of MC-algorithms is the law of great numbers which is a collection of mathematical propositions, which basically says that the relative frequency of a random solution stabilizes as a rule over the theoretical probability of a random experiment, if it is run all the time under same conditions and with a great number of repetitions. Even with a great repetition number there can be outliers, so it is a non-monoton approximation. The uncertainty of a Monte Carlo simulation is proportional to $1/\sqrt{N}$, whereby N is the number of histories. High performance random number generators are the basis of precise MC-algorithm results. All random number generators have a period, that is a number sequence repeating itself eventually. In modern codes the period number is long enough not to effect simulation results [11, p. 266].

MC-Simulations in Proton Therapy

Mathematically equivalent to solving the Boltzmann transport equation for protons in matter by using for example numerical Monte Carlo integration, is a randomly particle step-by-step simulation based on one or more probability distributions, representing probability of physics interaction and their outcome. These cross sections come from models like Molière's theory and experimental data, especially for nuclear reactions. The particle history, which is the knowledge of the trajectory of one particle including potential secondary particles, can be shown in a MC-simulation. For each step point physical properties of the material, like elemental composition, electron density, mean density and mean excitation energy must be known in order to choose how particle interact during a small step (be absorbed, annihilated, change density and energy, ...). The simulation outcome depends on the chosen step size, which should be small for a small cross section difference between the two step points, but not too small for decreasing computing time. Especially handling of the step size is necessary next to material boundaries. Because simulation of a huge number of single scattering events would take too long, class II condensed history algorithms were developed, which condense or sum energy loss and directional changes in a single step. Some codes define a δ-electron production threshold. Above this threshold δ-electrons are produced explicitly and below there is a continuous energy loss of primary particles. After this continuous energy loss a certain multiple scattering angle is assumed. The multiple Coulomb scattering is usually realized with a combination of continuous processes based on condensed history and discrete processes on explicit models for each interaction. In proton therapy these discrete processes are nuclear interactions, secondary particle production and large coulomb scattering.

2.7 TOPAS and Geant4

TOPAS (TOol for PArticle Simulation) is an extension based on the Monte Carlo toolkit Geant4 ("GEometry ANd Tracking 4"), which has the approach to be a less complex, reliable, repeatable and still a flexible and more user-friendly tool, specialized to proton therapy. TOPAS can model quantities such as passive scattering or scanning beam treatment heads, model a patient geometry based on CT (computed tomography) images, score dose and fluence, save and restart phase space. It provides advanced graphics and is fully four-dimensional (4D) to handle variations in beam delivery and patient geometry during treatment [7]. Initial TOPAS validation results show agreement with measured data at UCSF (University of Calafornia San Francisco Comprehensive Cancer Center) eye treatment head, MGH (Massachusetts General Hospital) stereotatic alignment in radiosurgery treatment head and MGH treatment heads, which are simulated in scattering and scanning modes [7]. Before describing the TOPAS structure, some facts about Geant4 are presented.

Geant4

Geant4 is the current version of a Monte Carlo simulation program from an international collaboration written in C++, which simulates the interaction of particles traversing in matter. It has applications in many areas of high-energy-physics with nuclear reactions like medicine and astrophysics. The source code is free, so everyone can modulate the program for his own applications. Geant4, which means "GEometry ANd Tracking 4", is divided into these two parts. It allows the administration of events, the scoring of detectors, a user interface and visualization. Geant4 is a so called toolkit, which means, that for every usage an application has to be created. A minimal simulation needs the definition of geometries and materials, an integration of physics with particles, models and processes and a run-manager. The integration of output formats and visualization is up to the user. With the possibility to model time dependent geometries, Geant4 is suited for intensity modulated radiation therapy in organ motion studies [8, 37-38].

Detector Geometry   The integration of detectors is realized with a world- construction-class, where at first a costructive-solid geometry model (CSG-model) is described and than provided with the physical properties of the materials. In the next step these geometries are placed in the Geant4-World and marked as a sensitive detector. Using Geant4 classes the program can write out all requested informations of the particles flying through the matter [8, p. 39] [5, p. 95].

Tracking   Geant4 uses for tracking the MC-principle of pre-step- and post-step-points, that are connected with one step. For a better code performance no continuous step length is used,

but a step length adjusted to the material, which can be, for example, in air or in vacuum much longer than in a scintillation material. The particle track is the sum of all steps, and for every step all information between the two points are calculated. For every calculation the volume and material for each point is defined and if a particle has on his post-step-point no more rest energy, the track is stopped and just decay processes can appear anymore. If a particle still has rest energy, the next step will be calculated. To avoid to jump over materials the post-step-point for steps with changing material is set on the border between current and next material/volume, and this point is addressed than to this next material/volume. The step length is limited to the process with the shortest interaction length. With the connection between two materials/volumes in one step, boundary processes like reflection, breaking, crossings or crossing radiation can be simulated [8, 38-39] [5, p. 172-175].

TOPAS Structure

TOPAS is a "user code" layered on top of Geant4 plus additional C++ code making Geant4 easier to control and extend its functionality. However, TOPAS will evolves if Geant4 evolves. The heart of TOPAS is the parameter control system, which allows the user to control geometry, particle source, fields, motion, scoring, graphical output and physical settings by constructing txt-files without the need of detailed knowledge of Geant4. Every command line in a txt-file has the same structure: "Parameter-Type:Parameter-Name = Parameter-Value" and the order of command lines does not matter. Every Parameter-Name has to be attached with a Parameter-Type to avoid user errors. Also every Parameter-Name has a corresponding major part. Example parameter settings with all types and major parts are listet in Figure 2.10.

- d:Ge/Phantom/HLX   = 10. cm   # Double
- u:Ge/Magnet/Dipole/DirectionX = 1.0   # Unitless Double
- i: Sc/DoseScorer/ZBins   = 100   # Integer
- b:Sc/DoseScorer/Active   = "True"   # Boolean
- s:Ge/Phantom/Material   = "Water"   # String
- dv:Ge/RMW_Track1/Angles = 4   69.11   92.29   111.04   126.02   deg   # Double Vector
- uv:Ma/Phantom_Plastic/Fractions=3 0.055491 0.755751 0.188758   # Unitless Double Vector
- iv:Gr/Color/yellow= 3 225 255 0   # Integer Vector
- bv:Tf/ScoringOnOff/Values=5 "true" "false" "true" "false" "true"   # Boolean Vector
- sv:Ma/PhantomPlastic/Components=3 "Hydrogen" "Carbon" "Oxygen" # String Vector

Figure 2.10: TOPAS example parameters [12, p. 5].

TOPAS supports relative parameters, where one parameter can be set relative to another. It is possible to add and multiply parameters if they have matching types. TOPAS has a built-in hierarchical control where other files can be included using "includeFile = someFile somOtherFile ..." and the parameters in the user file overwrite the parameters in the included file. At the end of this hierarchy there are the TOPAS default parameters. TOPAS checks,

that no two parameter file chains, that modify the same parameter, are defined in a way that is ambiguous.

There are default parameters for TOPAS overall control (like run-, event- or tracking verbosity or settings for showing the history), timeline control, optional checks, top level geometries, beam position, particle source, elements, materials, physics, scoring, colors and graphics, which can all be overwritten. A material is defined as shown in Figure 2.11.

- s:Ma/Air/Components="Carbon Nitrogen Oxygen Argon"
- uv:Ma/Air/Fractions=4 0.000124 0.755268 0.2317810 012827
- d:Ma/Air/Density=1.2048 mg/cm3
- d:Ma/Air/MeanExcitationEnergy=85.7 eV
- s:Ma/Air/DefaultColor=„lightblue"

- sv:Ma/Vacuum/Components=4 "Carbon" "Nitrogen" "Oxygen" „Argon"
- uv:Ma/Vacuum/Fractions=4 0.000124 0.755268 0.231781 0.012827
- d:Ma/Vacuum/Density=1.0E-25 g/cm3
- s:Ma/Vacuum/State="Gas"
- d:Ma/Vacuum/Temperature=2.73 kelvin
- d:Ma/Vacuum/Pressure=3.0E-18 pascal
- s:Ma/Vacuum/DefaultColor="skyblue"

- sv:Ma/Water/Components=2 "Hydrogen" "Oxygen"
- uv:Ma/Water/Fractions=2 0.111894 0.888106
- d:Ma/Water/Density=1.0 g/cm3
- d:Ma/Water/MeanExcitationEnergy=75.0 eV
- s:Ma/Water/DefaultColor="blue"

Figure 2.11: TOPAS default materials [12, p. 13-14]. The upper part of the figure shows the air definition, the center part the vacuum definition and the lower part the water definition in TOPAS.

Often, the TOPAS viewing mode is used in this bachelor thesis, which is described in subsection A.4. The particles can be colored by different features. In this work they are colored by their particle type. The default colors are shown in Table 2.2.

Particle	proton	neutron	photon	e-	e+	pi+-	other
Color	cyan	yellow	green	red	blue	magenta	grey

**Table 2.2:** TOPAS default particle colors.

3 Constructing TOPAS Examples

The scope and structure of TOPAS was introduced in the previous chapter and is discussed in detail in the Appendix (chapter A). This chapter supports this knowledge by discussing example applications and giving visual impressions. Basic geometries and special components are shown. For rebuilding them TOPAS txt input files are provided in the Appendix. Beam currents of protons, electrons, neutrons and photons in air are simulated and the observed interactions are discussed. The particles are colored by their type. The default colors are shown in Table 2.2.

3.1 Basic Geometries

The left plot in Figure 3.1 shows the three dividable components, that are elemental for scoring. More complex, but non-dividable geometry shapes (center plot) are implemented in Geant4 and can be used in TOPAS. Moving an entire block of geometries at the same time or rotating them is done by building components into parent components (right plot and Figure 3.2). The components in the parent are defined regarding the coordinate system of the parent and no more regarding the coordinate system of the world.
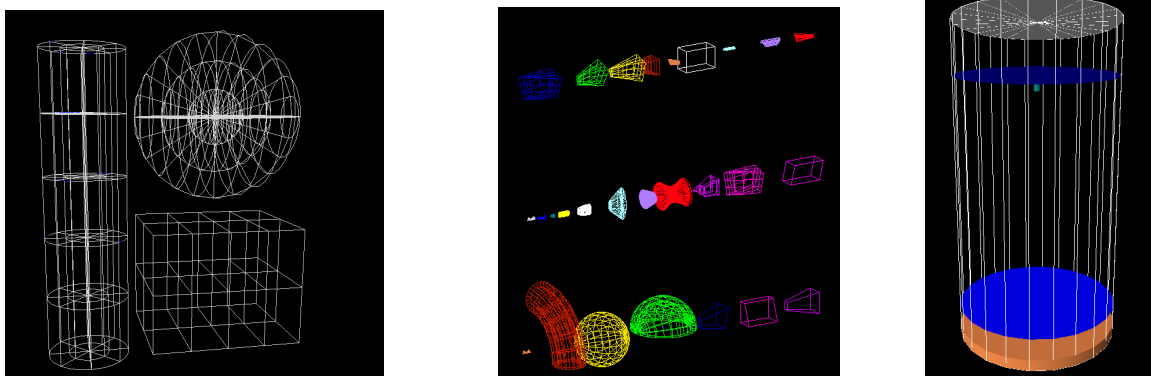
Figure 3.1: Basic TOPAS geometries. The left plot shows the three dividable components TsBox, TsCylinder and TsSphere. The center plot shows all Geant4 geometries, that can be used in TOPAS too. The right plot shows a cylindrical parent component including three foils starting from the bottom: brown, blue and blue and one green stopper between the two blue foils.
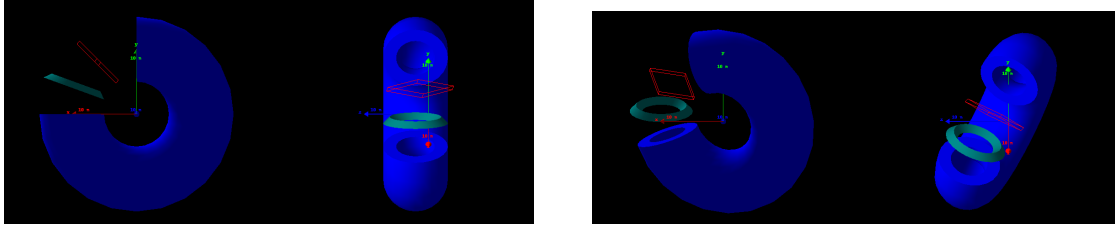
Figure 3.2: TOPAS group parent. A Geant4 torus (blue), a parallelogram (red) and a polycone (green) are defined in a group parent and in the right plot the group parent is rotated by 20° in X, Y and Z direction.

3.2 Special Components

Special components help to construct medical settings. Three special components are shown in this section: the range modulation wheel, dipole- and quadrupole magnets. More information can be found in the TOPAS User Guide [12, p. 31-58].

Figure 3.3 shows the construction of a range modulation wheel. It is vertically divided into three sections and each section can have its own steps. In addition a hub and a shell have to be defined. The upper section includes ten lexan blocks for range modulation, the middle section two disks (aluminum and lead) for blocking secondaries and the upper section eight lead blocks for scattering compensation. The hub and shell material is aluminum (Figure 3.3). Dipol- and quadrupole magnets can be built by constructing a mother volume like a TsBox and define the magnetic parameters, which are the strength and direction of the magnetic field. The left plot in Figure 3.4 shows a dipole box filled with air. The strength of the magnetic field is 1.0 Tesla and its direction vector $\vec{v} = (0.55|0.55|0.0)$. The particle color follows the Geant4 defaults: magenta-p, red-e^-, green-*gamma* and yellow-n. The right plot in Figure 3.4 shows two dipole magnets steering a 40 MeV proton beam, each by 90°, so the beam current points in the opposite direction. There are three quadrupole magnet boxes filled with air. All quadrupole fields are turned off, except for the last one, which has a strength of 0.9 tesla and a direction vector of $\vec{v} = (-1.0|2.0|3.0)$. The beam deflection of the charged protons in magnetic fields happens through the Lorentz force, which acts perpendicularly to the particle velocity vector and the magnetic field vector.

Figure 3.3: Construction of a range modulation wheel. The left plot shows a range modulation wheel without a shell and a hub to visualize the 10 lexan steps for range modulation in the upper section (left, white) and the corresponding lead steps at the bottom section (right, brown) for scattering compensation. The right plot includes an aluminum shell and an aluminum hub.
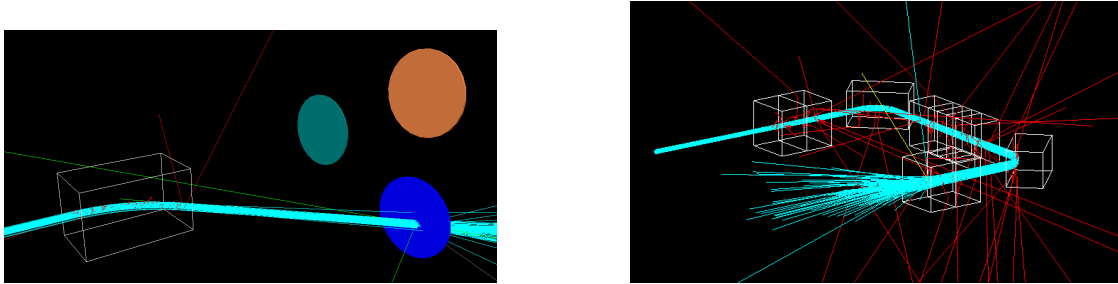
Figure 3.4: Dipole and quadrupole magnets steering a 40 MeV proton beam. In the left plot a dipole magnet steers a proton 40 MeV proton beam to a blue water cylinder. In the right plot dipole and quadrupole magnets are built together to deflect a 40 MeV proton beam. Only the quadrupole field of the last box is turned on. 100 primary protons are simulated in each plot.

3.3 Beam Currents

Figure 3.5 shows proton beams traversing through air. For the 10 MeV proton beam the secondary electrons, produced by Coulomb interactions have less kinetic energy and travels short distances away from the beam. The higher the proton beam energy, the longer is the secondary electron travel path length. This effect can be observed in air, because of the low air density. The main dose deposit happens through this secondary electrons. For the 10 MeV proton beam a beam widening can be observed. As the proton velocity component in beam direction shrinks, the velocity component perpendicularly to the beam increases for non-direct nuclei collisions, because of momentum conversation. For the 50 MeV beam the production of helium particles, neutrons and photons can be observed, which are produced in non-elastic collisions.
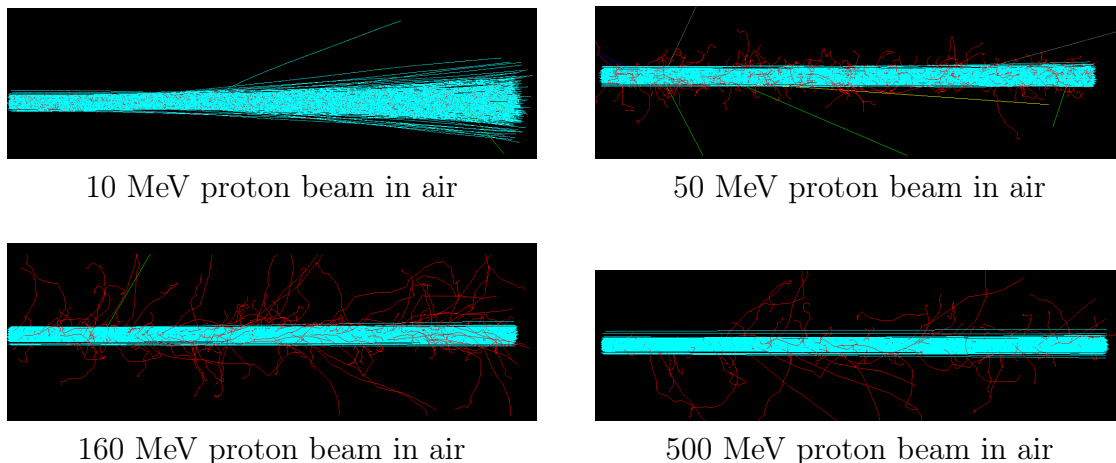
The beam widening of the 5 MeV electron beam in Figure 3.6 works after the same principle as the beam widening of the proton beam in Figure 3.5, except the scattering collisions are between electrons and not between nuclei. As electron energy increases, the scattering decreases.

Because air has a low density and basically consists out of nitrogen, oxygen and hydrogen, which have atomic numbers lower than eight, the interaction probability between photons and air atoms is small and 10,000 photons have to be simulated to observe interactions. The

basic interactions of photons in matter are: photo effect, incoherent scattering or pair/triplet production. For the 6 keV photon beam the photo effect is dominant. The photo-electrons have low energy and travel small distances making them hard to observe. But they can be observed indirectly through collisions with primary photons, which are hit out of the beam. For the 6 MeV photon beam incoherent scattering and pair production dominate. The produced electrons have momenta mainly in beam direction. In addition, the production of a proton can be seen, which probably results from the collision of a high-energy photon with the single electron of a hydrogen atom.
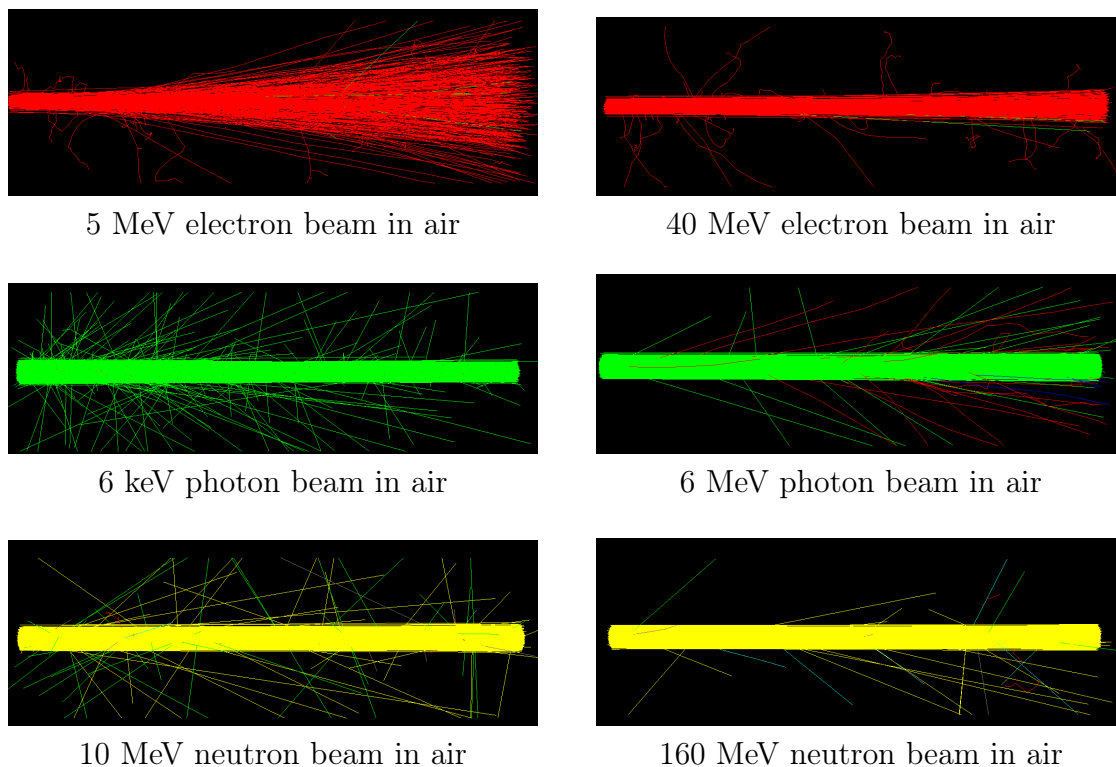
As photons, neutrons are uncharged particles with less interaction probabilities compared to electrons and protons. Therefore, 10,000 neutrons have to be simulated to observe interactions, that can be discussed. For lower neutron beam energies more photons can be observed, and for higher neutron energies more protons. Through non-elastic collisions with atomic nuclei the low-energy neutrons just stimulate the nuclei which emit high-energy photons. As neutron energy increases also protons can be knocked out of the nuclei. Elastic scattering with atomic nuclei can be observed, too. The higher the kinetic neutron energy, the more the scattering direction follows the beam direction.

TOPAS allows building any number of sources. By using beams coming from different directions a treatment planning optimization program, for example, has more free parameters to maximize the dose deposit in the tumor and minimize the dose deposit in the surrounding critical structures. Figure 3.7 shows 4 beams of different energies hitting a water target. Protons and alpha particles are compared. The energy per nucleon is constant. The different ranges in each plot can be observed. As the atomic number of the beam particle grows, the neutron production increases for equal dose deposit.

10 MeV proton beam in air   50 MeV proton beam in air

160 MeV proton beam in air   500 MeV proton beam in air

Figure 3.5: Proton beams in air. 4 proton beams with different energies in air. All beams have TOPAS default parameters (section A.2) and 300 primary protons are simulated.

5 MeV electron beam in air

40 MeV electron beam in air

6 keV photon beam in air

6 MeV photon beam in air

10 MeV neutron beam in air

160 MeV neutron beam in air

Figure 3.6: Electron, photon and neutron beams in air. The upper plots show two electron-, the center plots two photon- and the lower plots two neutron- beams traversing in air. The beams have different energies. All beams have TOPAS default parameters (section A.2). For the electron beams 300 primary particles are simulated, for the photon and neutron beams 10,000 primary particles.
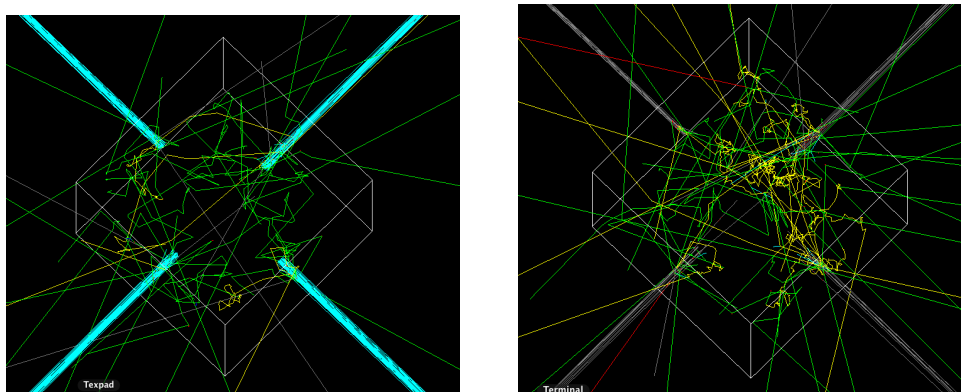
Figure 3.7: 4 proton and 4 alpha particle beams hitting a water target. The cubic water target has a side length of 60 cm. The beam energies per nucleus are: 80MeV/nucleus-upper left beam, 100MeV/nucleus-bottom right beam, 120MeV/nucleus-bottom left beam and 140MeV/nucleus for the upper right beam. All beams have TOPAS default parameters as shown in section A.2, except their circle shape is 3 times larger (radius=30 cm). 40 primary protons are simulated and 10 primary alpha particles for each single beam, so dose deposit is equal.

4 Simulations in a Water Phantom

The next two chapters will examen TOPAS performance in describing energy loss in matter and multiple Coulomb scattering. The proton ranges in water will be compared with PStar (NIST) data and the scattering results with Highland's formula. Additionally, the construction and the scoring of settings with increasing complexity prepare the analysis of the IBA gantry and deliver different topics to discuss.

To discuss physical advantages and disadvantages of proton therapy compared with photon- and heavier ion therapy, depth-dose-curves of photons and alpha particles will be scored. The construction of spread out Bragg peaks by direct modulation of the beam energy and passive modulation by using a range modulation wheel will be introduced at the end of this chapter. Both modulation techniques are implemented through TOPAS time functions (subsection A.4).

For the simulations in all chapters following TOPAS default beam parameters are used which are shown in section A.2. The particles are colored by their type. The default colors are shown in Table 2.2.

4.1 Depth-Dose-Curves

Construction and Simulation

The 1D depth-dose-curves are scored in a cylinder divided into z-bins and the 2D depth-dose-distributions are scored in a box divided into x- and z-bins. A cylindrical scorer can exploit the cylindrical beam symmetry. This is especially important for range analysis. The more qualitative 2D depth-dose-distributions show the beam in the full vertical range, which would be more difficult by using a cylindrical scorer. In addition, the quadratic scorer corresponds to the experimental way of measuring lateral profiles through ionization chambers with small volumes. Figure 4.1 shows the basic setting, which is used for scoring the deposited dose of protons, alpha particles and photons. To compare the proton and alpha beam the energy per nucleon is the same. For the 1D photon depth-dose-curve a clinical relevant energy of 6 MeV is used. The curve is compared with a proton spread out Bragg peak in the introduction chapter (Figure 1.1).
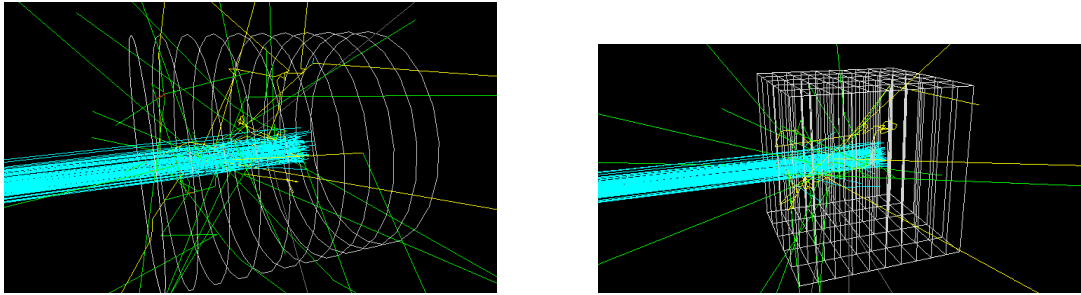
Figure 4.1: Settings for the depth-dose-curve simulations. The left plot shows the setting for the simulation of 1D depth-dose-curve . The cylindrical water scorer (radius=10 cm, length=20 cm) is divided into 10 z-bins. The right plot shows the setting of the simulation of 2D depth-dose-distributions . The cubical water scorer (length=20 cm) is divided into 10 z- and 5 x-bins. The proton beam has an energy of 140 MeV and TOPAS default parameters. 100 primary protons are simulated.

Results

The simulated depth-dose-curves are analyzed and visualized with Python. The dose values are normalized to the maximum dose. The maximum dose D_{max} is set to 100:

$$D[\%] = 100 \cdot \frac{D}{D_{max}} \tag{4.1}$$

The relative dose D_{rel} is given in percentage of the maximum dose. TOPAS scores always the dose per primary particle number, which depends on the simulated histories.

Figure 4.2 shows an example of a Bragg peak corresponding to the setting in Figure 4.1. For four characteristic dose values, the maximum dose, 90%, 80% and 20% of the maximum dose after the maximum and the ranges are calculated and compared with PSTAR data (Figure 4.3). The depth-dose-curve corresponds to the expected behavior, which is a Bragg peak with a sharp maximum and a short fall-off. The fall-off region increases for higher energies as it can be observed in the increasing point distances in Figure 4.3. The TOPAS simulated range values of $R_0=R_{0.8}$, where half of the protons have been stopped, lie on the PSTAR energy-range-curve for the studied energy interval.
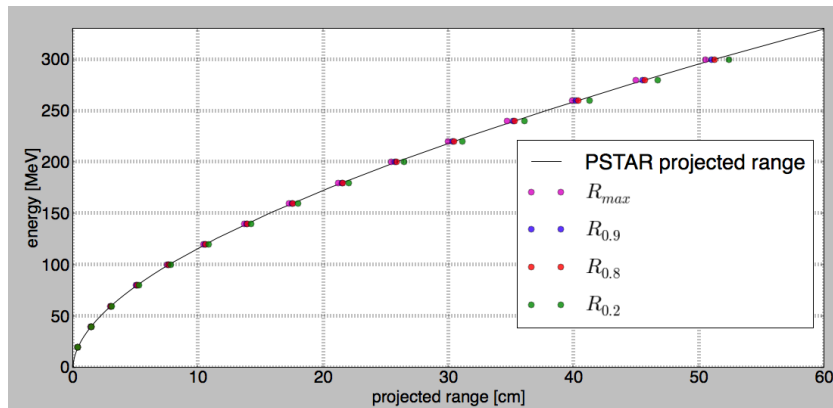
Figure 4.4 shows the 2D depth-dose-distributions and neutron fluence distributions of protons and alpha particles. The number of simulated protons is four times higher than the one of the alpha particles, so the dose deposit is equal. The lateral spread of the proton beam is larger, and the neutron production lower compared to the alpha particles. The lateral spread of both beams increases with depth. The maximum dose is deposited at the distal end of the Bragg peak.

Figure 4.5 shows the 2D depth-dose-distributions of a 6 MeV and a 15 MeV photon beam. The monoenergetic beams have a circular shape (radius=0.5 cm). The two beams differ in their
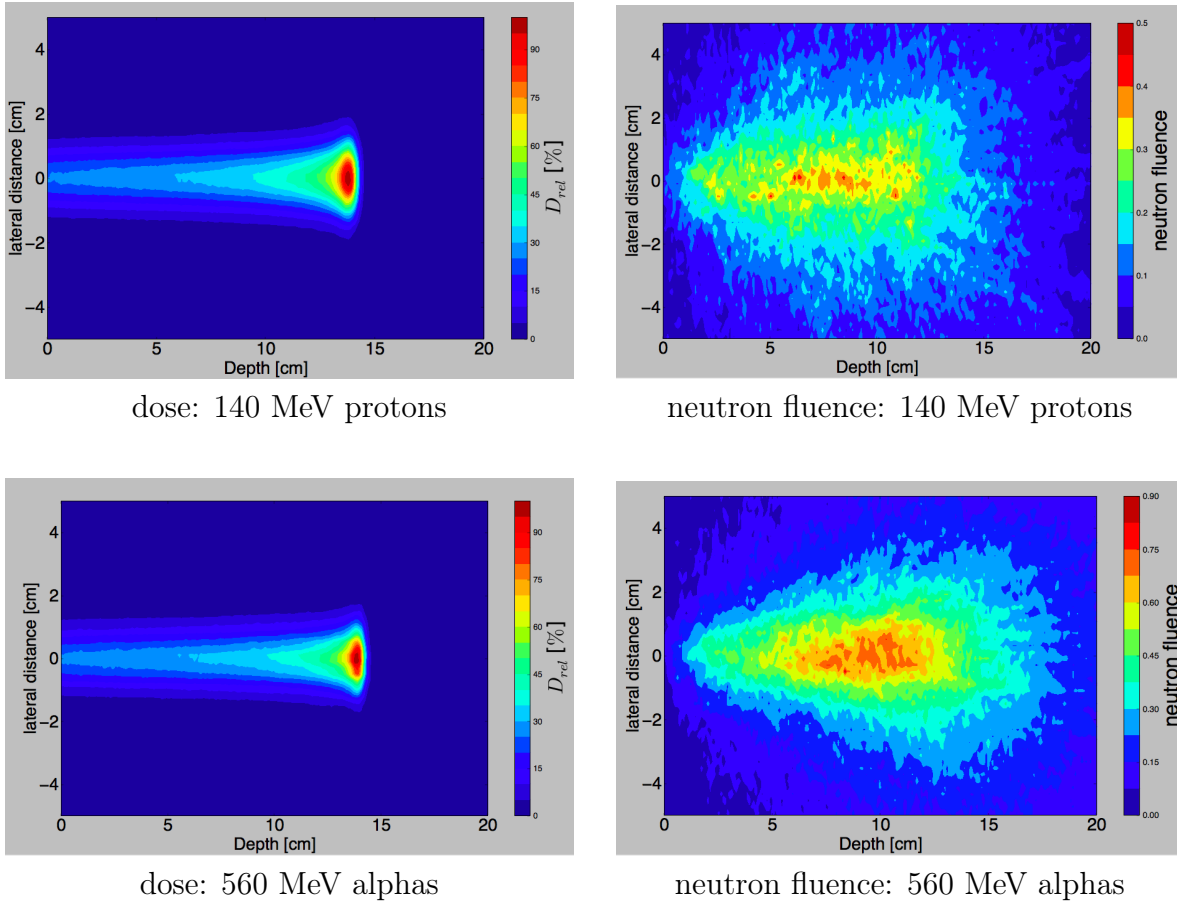
dose build-up and dose fall off. The 6 MeV photon beam deposits its maximum dose at lower ranges and the dose fall-off is stronger compared to the 15 MeV photon beam. The lateral profile spreads stay almost constant and the lateral spread differences between the two beams are ≤ 1 mm.
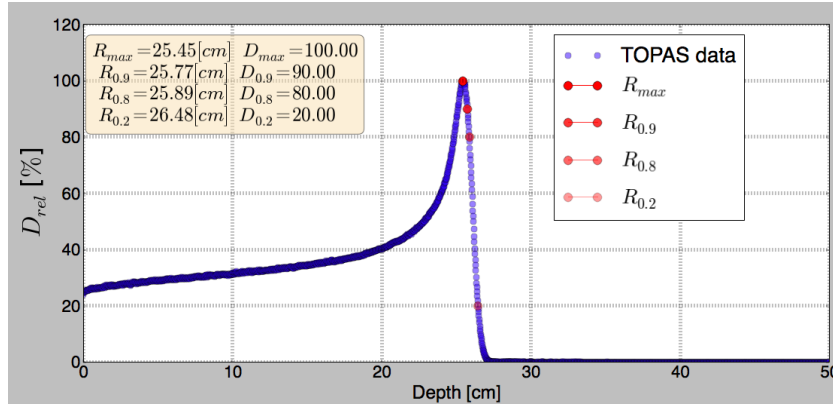

Figure 4.2: 200 MeV proton Bragg peak. Bragg peak of a 200 MeV proton beam in water (corresponding to Figure 4.1). The cylinder scorer size is increased to 60 cm. 10^5 primary protons are simulated and scored in 3000 bins.

Figure 4.3: Comparison of TOPAS and PSTAR proton beam ranges. The calculation of the ranges is shown in Figure 4.2. For eight different beam energies the ranges of the maximum peak R_{max}, and of 90%, 80% and 20% of the maximum peak $R_{0.9}$, $R_{0.8}$ and $R_{0.2}$ are compared with data from PSTAR (NIST) [10].

dose: 140 MeV protons   neutron fluence: 140 MeV protons

dose: 560 MeV alphas   neutron fluence: 560 MeV alphas

Figure 4.4: 2D depth-dose-distributions and neutron fluence distributions of protons and alpha particles. The proton beam energy is 140 MeV and the alpha particle beam energy is 560 MeV. The simulation setting is shown in Figure 4.1. Dose and neutron fluences are scored in 100 x-bins and 200 z-bins. $4 \cdot 10^4$ primary protons and 10^4 primary alpha particles are simulated to obtain a similar dose deposit and to compare neutron fluences.

dose: 6 MeV photons   dose: 15 MeV photons
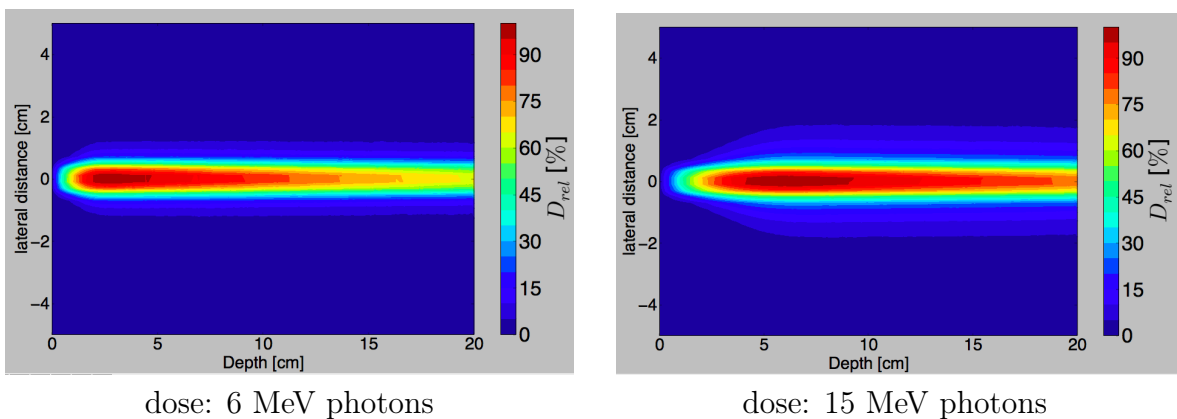
Figure 4.5: 2D depth-dose-distributions of a 6 MeV and a 15 MeV photon beam. The simulation setting is shown in Figure 4.1. The dose is scored in 100 x-bins and 200 z-bins. $5 \cdot 10^6$ photons are simulated for the 6 MeV plot and 10^7 for the 15 MeV plot. The photon beams have a circular shape (radius=0.5cm) and flat distributions.

4.2 Spread Out Bragg Peak

Construction and Simulation

The range modulation through direct beam energy modulation is done by using the setting shown in Figure 4.1 and adding a step time function (A.4). The range modulation through a range modulation wheel is shown in the three plots of Figure 4.6. Each plot is created on a different time interval and range step. The range step heights are 75 mm, 40 mm and 2 mm. 100 primary protons are simulated. The water cylinder is divided into 10 z-bins for 1D depth-dose-curves. The range modulation wheel includes an aluminum shell (Rin/Rout=15/15.5 cm) and an aluminum hub (Rin/Rout=6/7 cm). The length of the upper section is 15 cm, of the middle section 0.1 cm and of the bottom section 0.9 cm. The range modulation wheel is not scattering compensated and has just one very thin ($1 \cdot 10^{-4}$ mm) lead step in the bottom section. The lexan range modulation steps on the upper section can be changed by shape and number, depending on the spread out Bragg peak shape that should be created.

| step height 75mm | step height 35mm | step height 2mm |
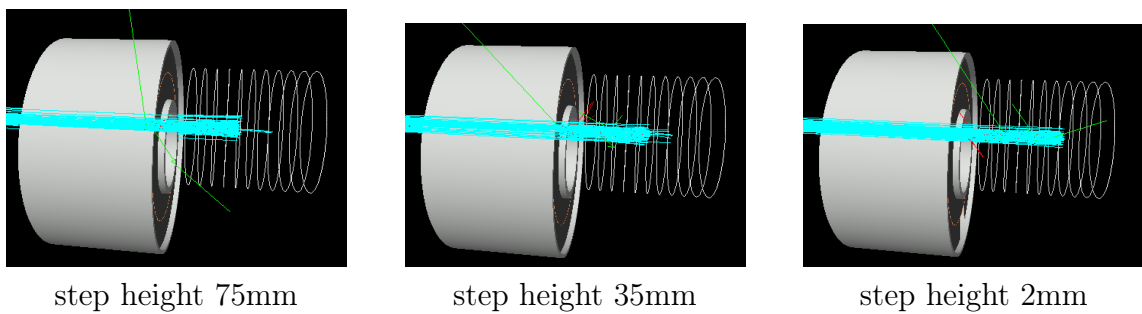
Figure 4.6: Setting for the simulation of a spread out Bragg peak with a range modulation wheel. A proton beam of 140 MeV entering first, a range modulation wheel and second a water cylinder (radius=10cm, length=20cm) from the left side.

Results

Two spread out Bragg peaks are scored using direct beam energy modulation. The first one is composed out of 6 Bragg peaks with energies between 150 and 160 MeV 2 MeV energy steps. The second one uses 13 Bragg peaks with energies between 100 MeV and 160 MeV and 5 MeV energy steps. There are more ripples on the 13-steps-spread out Bragg peak than on the 6-steps one. The ripples can be observed vertically and laterally. To understand the spread out Bragg peak construction the Bragg peak base with the corresponding weights is shown. The normalization is done using the time interval length of the step for the largest range.

In range modulation using a range modulation wheel ripples are observed, too. A spread out Bragg peak based on 4 Bragg peaks is constructed by using 3 lexan steps and one step with no material. To illustrate the spread out Bragg peak construction it is shown how the spread out

Bragg peak is built out of the Bragg peaks by decreasing the irradiated number lexan steps of the range modulation wheel. A linear time function controls the rotation of the wheel. It rotates with 3.6 deg/ms. Both optimizations are done in this study by hand.

More detailed information of time functions in TOPAS are described in the appendix in subsection A.4.

150-160 MeV proton   100-160 MeV proton
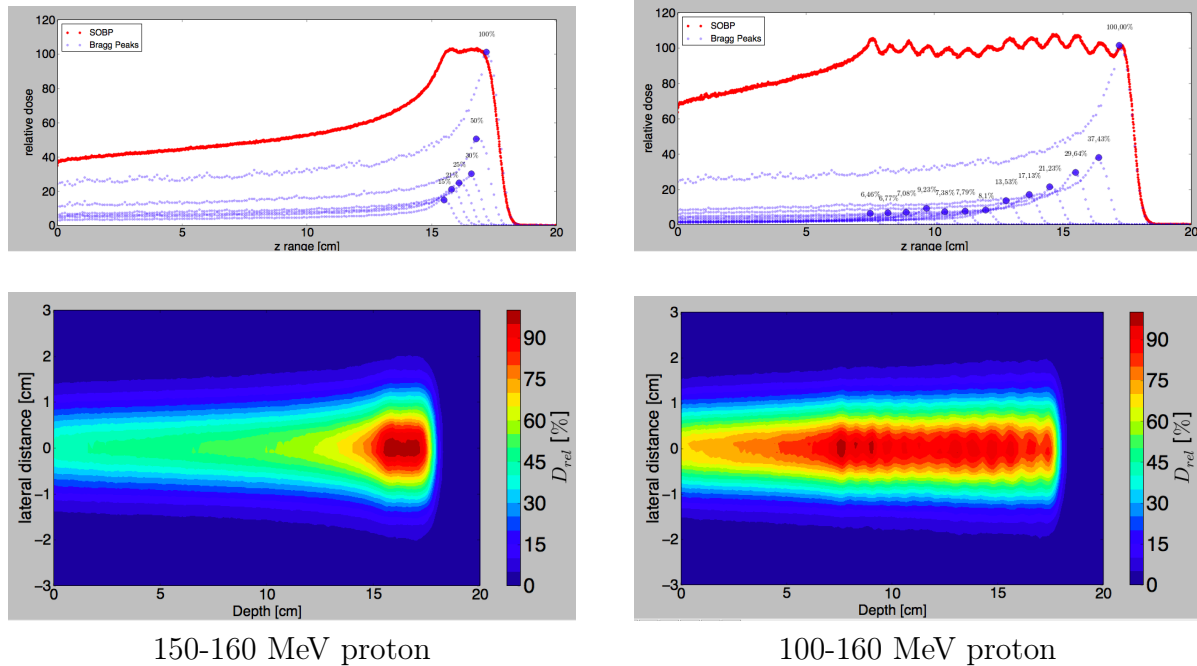
Figure 4.7: Construction of spread out Bragg peaks with direct energy modulation. The two left plots show the 1D depth-dose-curve and 2D depth-dose-distribution of a spread out Bragg peak constructed by using 6 different modulation widths. The pristine peaks have energies between [150|160] MeV and 2 MeV energy steps. The two right plots show the 1D depth-dose-curve and 2D depth-dose-distribution of a spread out Bragg peak constructed by using 13 different modulation widths. The pristine peaks have energies between [100|160] MeV and 5 MeV energy steps. 10^5 primary protons are simulated.
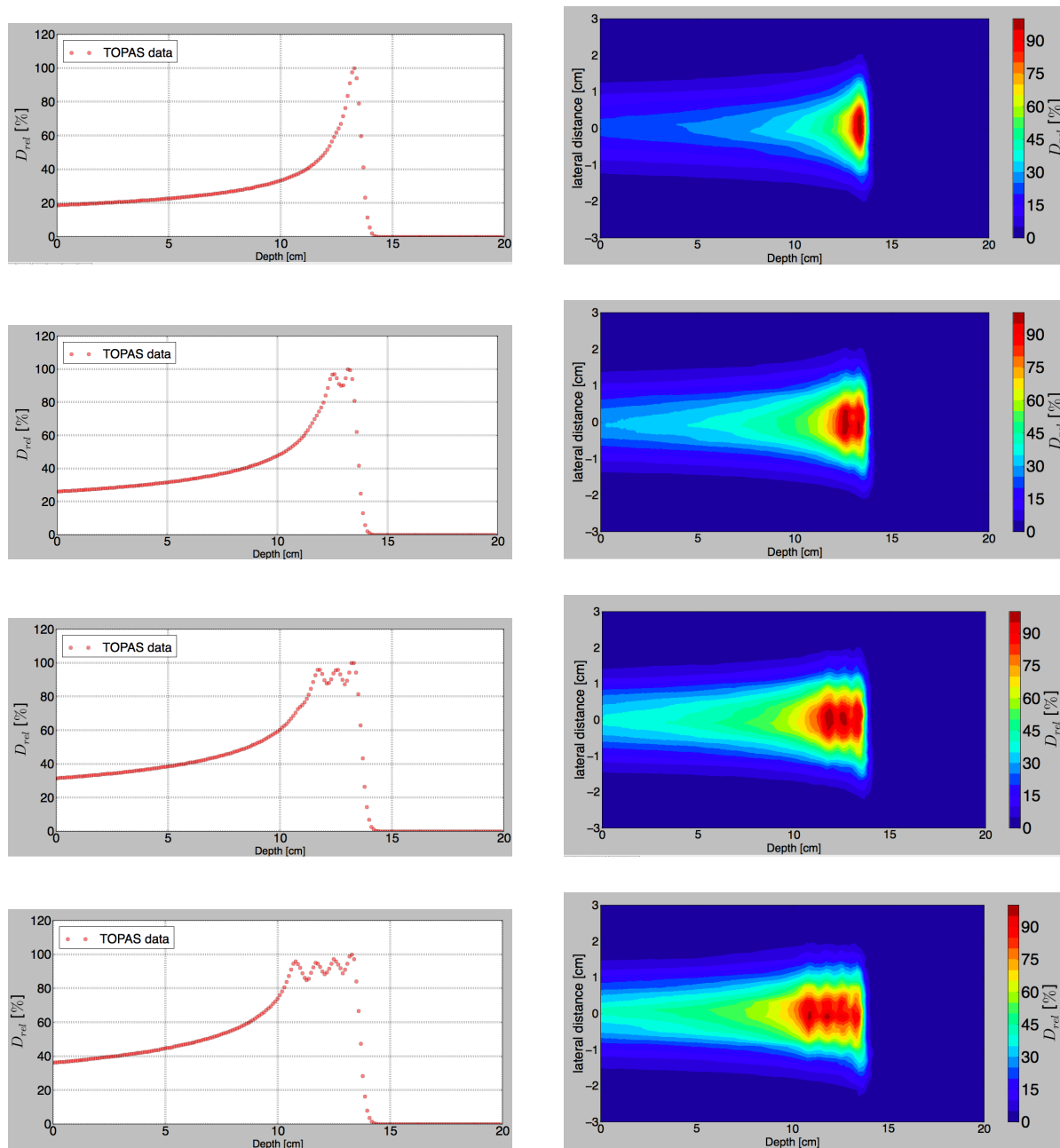
Figure 4.8: Construction of a spread out Bragg peak with a range modulation wheel. By decreasing the irradiated number of lexan range steps from 3 steps to 0 steps the modulation width of the spread out Bragg peak can be varied. The simulation setting is described in Figure 4.6. For the 1D- depth-dose-curves dose is scored in 200 z-bins and for the 2D- depth-dose-distributions the dose is scored in 100 x-bins and 200 z-bins. The wheel's angular rotation is 3.6 deg/ms and one full rotation is simulated in 100 time steps. For each time step 100 primary protons are simulated.

5 Scattering Systems

This chapter focuses on multiple Coulomb scattering. First, the agreement between Highland's formula and TOPAS will be analyzed for lead, copper, aluminum and lexan. Second, an eye treatment beam line, similar to the Clatterbridge beam line, will be constructed. Its profile in lateral and beam direction and the neutron fluences will be scored along the beam line and discussed. Taking the Clatterbridge double scattering system as a role model, a new scattering setting is constructed with the goal to get an enlarged homogeneous lateral profile (at least a circle of 5cm radius) for future cell irradiation experiments at Oncoray.

5.1 Single Scattering

Construction and Simulation

Figure 5.1 shows the single scattering setting. It includes a quadratic scatter foil (x|y length 40 cm) and a water cylinder target (thickness=1 cm), which is placed at a distance of L=2 m behind the foil. The water dose scorer is chosen, to increase the comparability of the single scattering setting with the setup for cell irradiation experiments. Effects of multiple Coulomb scattering in the water itself are negligible as discussed in subsection 7.3. The cylindrical scorer radius is adjusted to the scatter thickness to save scoring and simulation time. The r-bin size stays always 1mm. The 160 MeV proton beam has TOPAS defaults (section A.2). The scatter thickness d_S is varied for the four materials: lead, copper, aluminum and lexan. The lateral profile is Gauss fitted with a Python curve fitting module and the angle Θ_0 can be calculated from the the root mean square (rms).

$$rms = X_0 = \sqrt{\mu^2 + \sigma^2} \qquad \Theta_0 \approx \tan(\Theta_0) = \frac{X_0}{L} \text{ [rad]} \tag{5.1}$$

$$L = 2 \text{ m... distance between scatterer and scorer} \tag{5.2}$$

For the theoretical Highland curve (equation 2.8), the kinetic term pv for the beam energy (equation 2.11) and the radiation length L_R of each material (equation 2.12) have to be calculated. The material parameters are shown in Table 5.1.

Material	Z	A	$\rho \left[\frac{g}{cm^3}\right]$	$L_R \left[\frac{g}{cm^2}\right]$	$R_0 \left[\frac{g}{cm^2}\right]$
Lead	82	207	11.342	6.3	35.89
Copper	29	63.5	8.92	13.15	26.5
Aluminum	13	27	2.7	24.28	22.66
Lexan	6.23	11.56	1.19	40.55	18.11

Table 5.1: Material parameters as used for single scattering. Z is the nucleus charge, A the atomic number, ρ the density and L_R the radiation length of the scatterer material. R_0 is the projected range of a 160 MeV proton beam in the scatter material. NIST data are used.

$d_S = 1$ mm, E=50 MeV

$d_S = 1$ mm, E=200 MeV

$d_S = 0.2$ mm, E=160 MeV

$d_S = 10$ mm, E=160 MeV
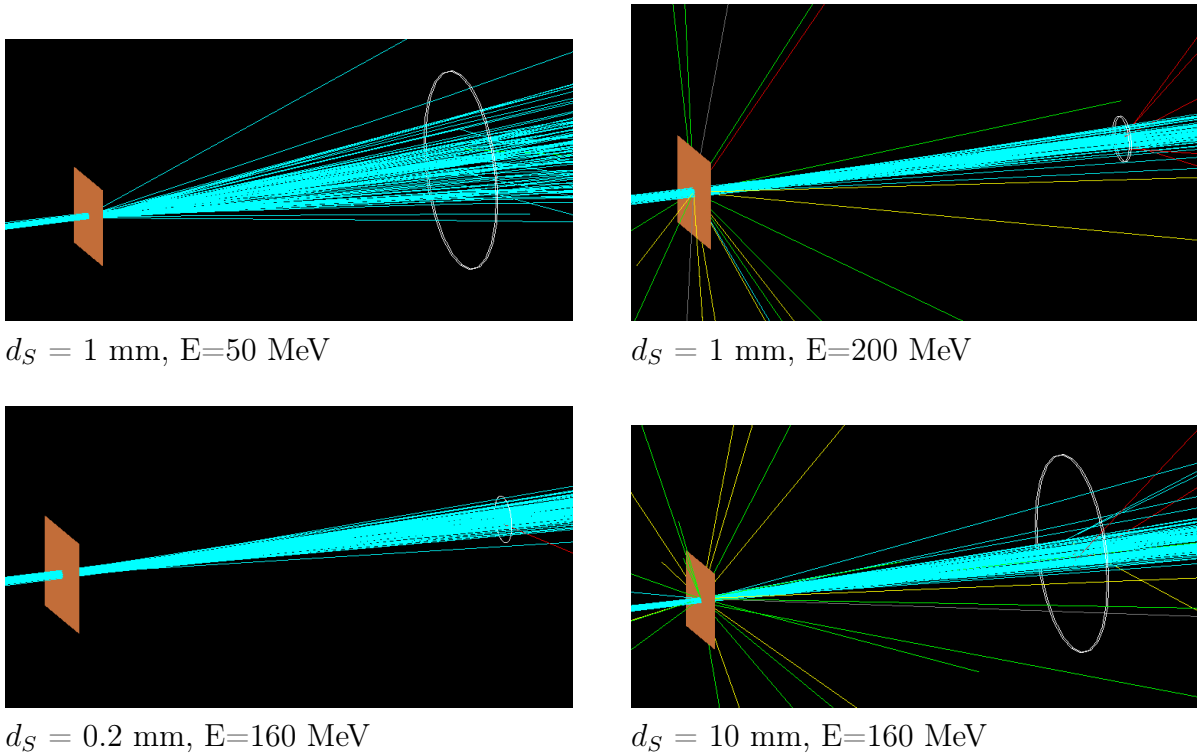
Figure 5.1: Single scattering of a proton beam on a lead foil. The effect of varying energy (upper row) and scatterer thickness (lower row) on multiple Coulomb scattering of a proton beam is illustrated. Lead is used as the scatterer material. The cylindrical water scorer has a thickness of 1 cm and a varying radius adjusted to the scatter thickness to limit scoring and simulation time.

Results

Figure 5.2 shows two lateral dose profile for lead scatterers including Gaussian fits. This fitting approach works well over the chosen energy and thickness intervals. The simulated and calculated values of Θ_0, for varying proton energy and varying scatter thickness, are listed in the Tables 5.2 and 5.3, respectively. The tables include the corresponding scatter thicknesses d_0 and the relative scatter thicknesses $d_{rel}=d_S/R_0$. d_{rel} is the scatter thickness normalized by the projected range R_0 of the proton beam in the scatter material with the chosen energy.

Table 5.2 corresponds to the upper plot in Figure 5.3 and shows TOPAS and Highland Θ_0-values of a single lead scatterer for energies between 50 MeV and 200 MeV holding the scatterer thickness of 0.1 cm constant. The simulated $\Theta_0(E)$-points and the calculated $\Theta_0(E)$-curve are shown in a double-logarithmic plot. Fixing scatter thickness at 0.1 cm the lateral profile broadens as beam energy decreases. For proton beam energies in the interval [100|200] MeV, the multiple Coulomb scattering angle differences between TOPAS simulations and Highland's formula are $\leq$ 2 mrad.

The lower plot in Figure 5.3 compares $\Theta_0(d_{rel})$- points simulated with the TOPAS and the $\Theta_0(d_{rel})$- curve calculated by Highland's formula in a double-logarithmic plot. Fixing beam energy at 160 MeV and varying scatter thicknesses, the width of the Gaussian profile increases as scatter thickness increases. The resulting differences are: $\Delta\Theta_0 \leq 3.3$ mrad (lead, $d_0 \in$ [0.02|1.0] cm); $\Delta\Theta_0 \leq 3.61$ mrad (copper, $d_0 \in$ [0.02|1.0] cm); $\Delta\Theta_0 \leq 3.04$ mrad (aluminum, $d_0 \in$ [0.06|1.0] cm); $\Delta\Theta_0 \leq 3.68$ mrad (lexan, $d_0 \in$ [0.1|6.0] cm). The intervals with minimal multiple Coulomb scattering angle differences are different for the four materials.

Lateral profile (Pb $d_S = 0.2$ mm)   Lateral profile (Pb $d_S = 1$ cm)
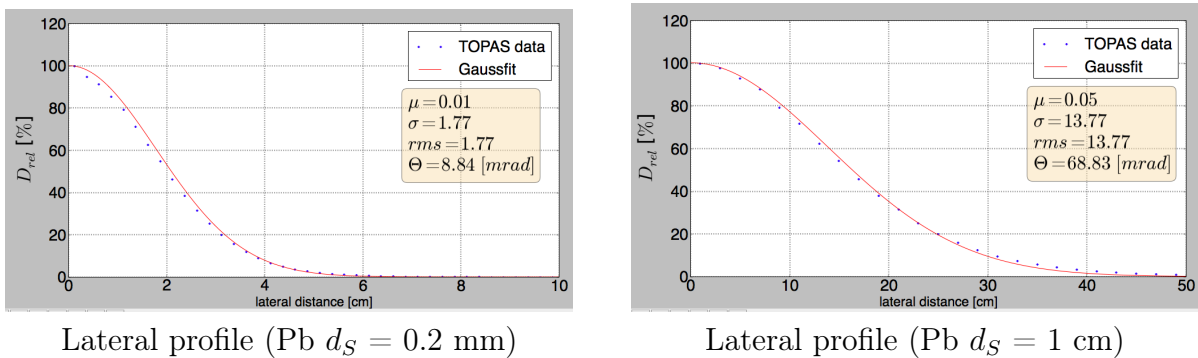
Figure 5.2: Lateral profiles with Gaussian fits. The proton beam has an energy of 160 MeV and the set-up corresponds to Figure 5.1. 10^6 primary protons are simulated.
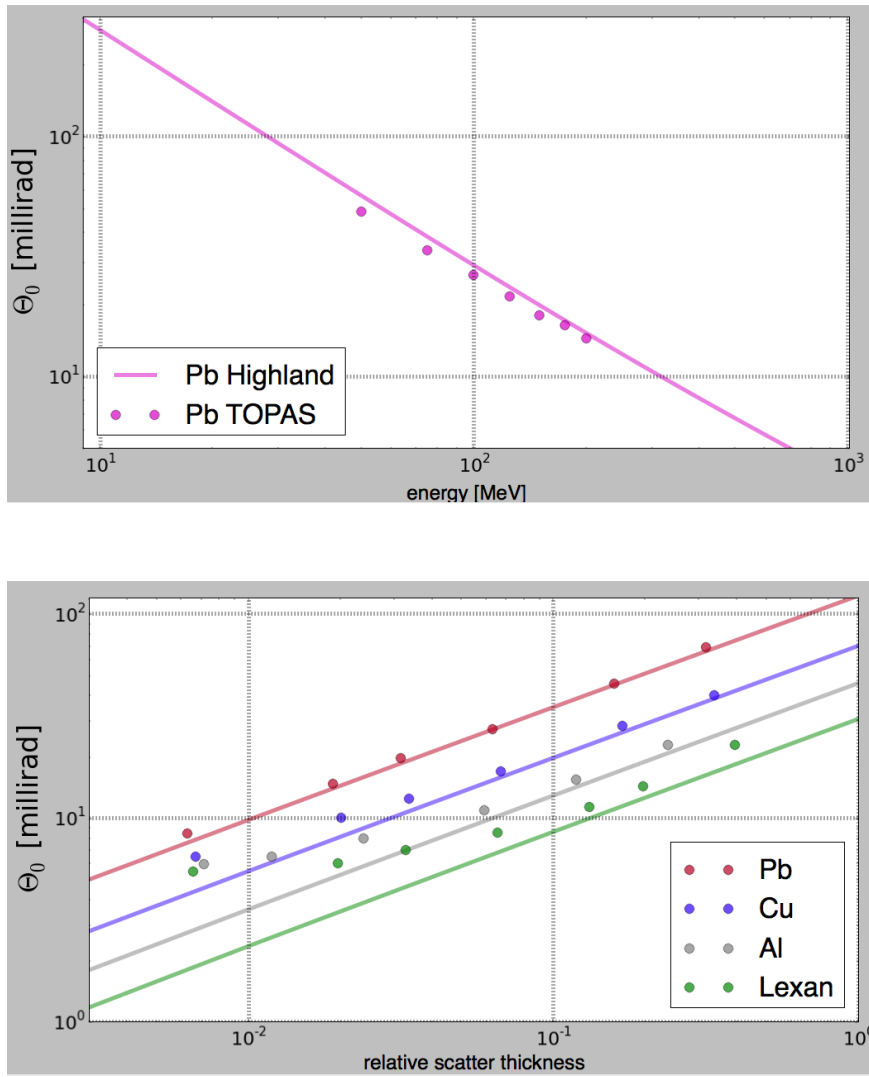
Figure 5.3: Comparison of the analytic $\Theta_0(E)$- and $\Theta_0(d_{rel})$-curve with TOPAS data. The setting of Figure 5.1 is used. The $\Theta_0(E)$-points (upper plot) are simulated by holding the lead scattering foil thickness constant to 1 mm. The $\Theta_0(d_{rel})$-points (lower plot) are simulated by holding beam energy constant to 160 MeV. 10^6 primary protons are simulated for each point.

energy [MeV]	50	75	100	125	150	175	200
d_S [cm]	0.1	0.1	0.1	0.1	0.1	0.1	0.1
d_S/R_0	0.23	0.11	0.07	0.05	0.04	0.03	0.02
Highland Θ_0 [mrad]	56.28	37.98	28.82	23.31	19.64	17.00	15.03
Θ_0 [mrad]	49.02	33.71	26.47	21.62	18.09	16.47	14.43
Θ_0 [deg]	2.81	1.93	1.52	1.24	1.04	0.94	0.83

Table 5.2: Θ_0 for different proton beam energies traversing a lead scatterer. Fixing the scatter thickness at 0.1 cm seven proton beams of different energy are simulated. The primary proton number for each beam is 10^6.

Lead						
d_S [cm]	0.02	0.06	0.1	0.2	0.5	1.0
d_S/R_0	0.0063	0.019	0.032	0.063	0.158	0.316
Highland Θ_0 [mrad]	7.57	13.94	18.49	27.1	44.84	65.55
TOPAS Θ_0 [mrad]	8.84	14.77	19.69	27.3	45.95	68.83
TOPAS Θ_0 [deg]	0.57	0.85	1.13	1.56	2.63	3.94
Copper						
d_S [cm]	0.02	0.06	0.1	0.2	0.5	1.0
d_S/R_0	0.0067	0.02	0.034	0.067	0.168	0.337
Highland Θ_0 [mrad]	4.39	8.1	10.77	15.82	26.23	38.4
TOPAS Θ_0 [mrad]	7	10.06	12.49	17.01	28.49	40.01
TOPAS Θ_0 [deg]	0.4	0.58	0.72	0.97	1.63	2.3
Aluminum						
d_S [cm]	0.06	0.1	0.2	0.5	1	2
d_S/R_0	0.0071	0.012	0.024	0.06	0.12	0.24
Highland Θ_0 [mrad]	2.94	3.92	5.79	9.64	14.17	20.79
TOPAS Θ_0 [mrad]	5.98	6.48	7.98	10.95	15.46	22.9
TOPAS Θ_0 [deg]	0.34	0.37	0.46	0.63	0.89	1.31
Lexan						
d_S [cm]	0.1	0.5	1	2	3	6
d_S/R_0	0.0066	0.02	0.066	0.13	0.2	0.39
Highland Θ_0 [mrad]	1.82	3.38	6.64	9.77	12.24	19.56
TOPAS Θ_0 [mrad]	5.5	6.97	8.51	11.41	14.41	22.9
TOPAS Θ_0 [deg]	0.32	0.4	0.49	0.65	0.83	1.31

Table 5.3: Θ_0 for different scatter thicknesses and materials. For lead, copper, aluminum and lexan scatterers of varying thicknesses the TOPAS and Highland Θ_0- angles are listed with the corresponding relative scatter thicknesses d_S/R_0. The proton beam energy is 160 MeV.

5.2 Clatterbridge Beam Line

Construction and Simulation

The Clatterbridge eye treatment beam line works with two flat scatterers and a stopper in between as schematically despited in Figure 5.4. The beam line is designed and optimized for protons of 62.2 MeV and a circular beam with 3 mm radius and a flat beam distribution. The range modulation wheel includes 33 PMMA (plexiglas) range modulation steps distributed over 45 deg. For beam analysis three vacuum scorers are built-in at representative positions (Scorer1|z=-28cm, Scorer2|z=40cm and Scorer3|z=179cm) and proton and neutron fluence is scored. The first two scorer positions are before and after the double scattering system. The third scorer is positioned before the water target. The range modulation wheel rotates linear with 0.5 deg/ms. The simulation time ends after 90 ms, so every step of the range modulation wheel is used. For every angle step 10,000 primary protons are simulated, so for every simulation $9 \cdot 10^5$ primary protons are simulated.
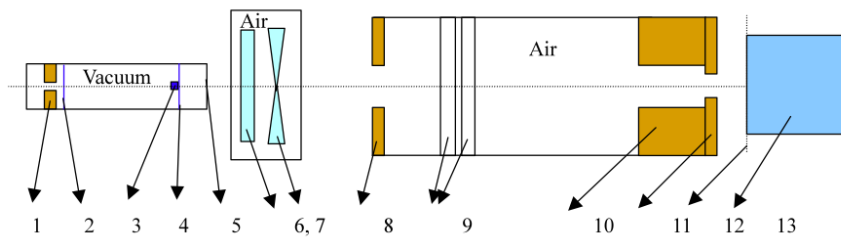

1. Pre-collimator (1.0 cm brass, 0.3 cm radius, z =-25.6)
2. Scattering foil (0.0025 cm tungsten, z = -22.6)
3. Stopper (0.66 cm brass, 0.2855 cm radius, z = -0.66)
4. Scattering foil (0.0025 cm tungsten, origin of geometry coordinates, z = 0)
5. Kapton window (0.005 cm thick, z = 5.0)
6. Range shifter (pmma, as appropriate, z = 27.0)
7. Modulator wheel (pmma, as appropriate, z = 27.0)
8. Collimator (1.0 cm brass, 2.0 cm radius, z = 55.0)
9. Ion chamber (0.002 cm mylar, 0.0004 cm Al, z = 115.0)
10. Collimator + nozzle (7.8 cm brass, 1.7 cm radius, z = 175.0)
11. Collimator (0.8 cm brass, square field definition, z = 182.8)
12. Reference plane (z = 184)
13. Water or graphite phantom (z = 184)

Figure 5.4: Clatterbridge construction plan. Construction plan of the Clatterbridge beam line with geometry parameters and positions. The double scattering system consists of two thin tungsten scattering foils, with a brass stopper in front of the second foil. The stopper scatters protons out of the center to reach a more homogenous profile. The range modulation wheel serves as a scatterer, too.

A graphical representation of the geometrical implementation of the Clatterbridge beam line in TOPAS is given in Figure 5.5. The positions of the three scorers are shown in the center plot. Also, the beam characteristics of the 62.2 MeV proton beam within the beam line are illustrated.
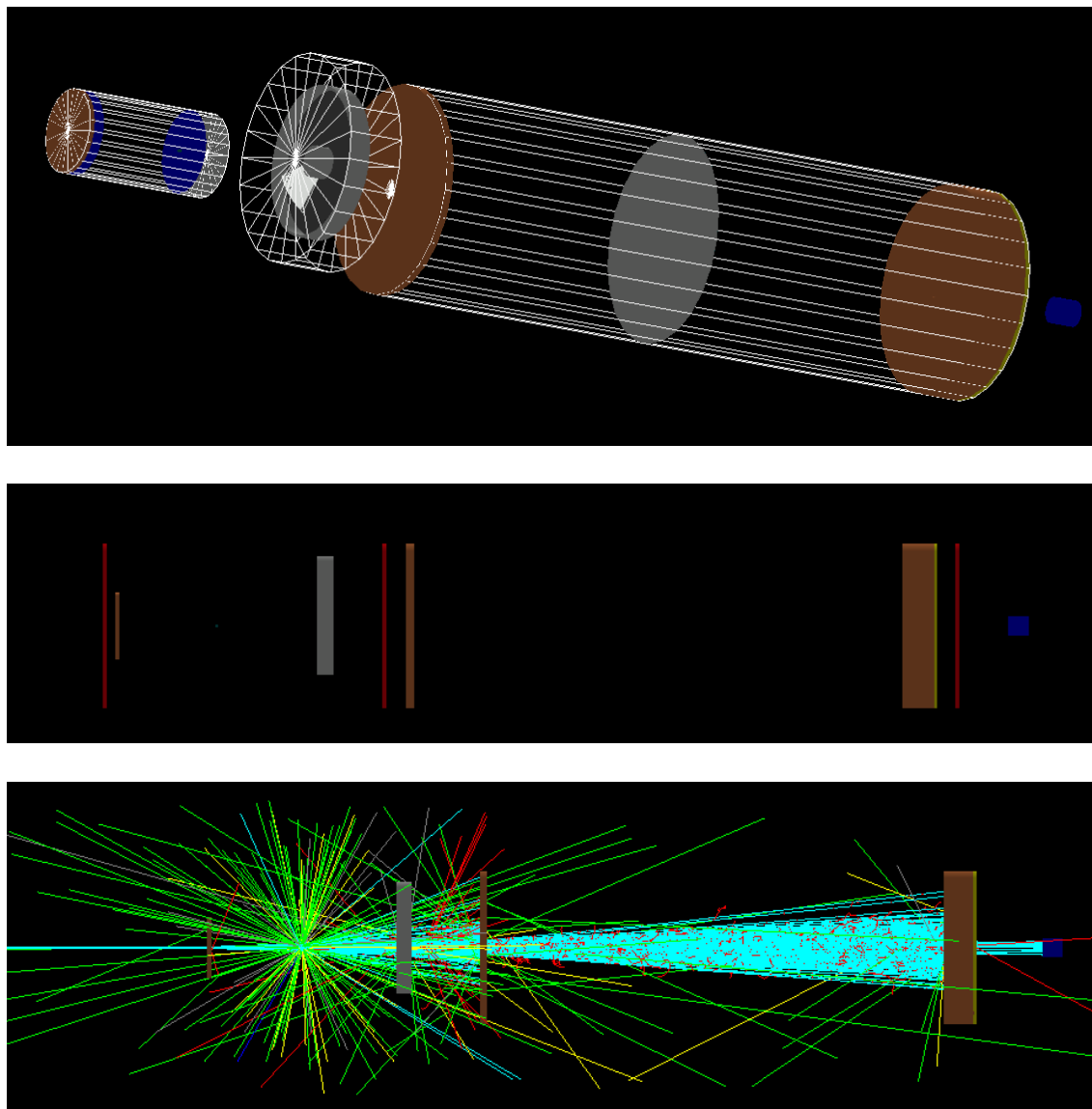
Figure 5.5: Clatterbridge beam line in TOPAS. The upper plot show all Clatterbridge components built into 3 parent chambers (white wireframe). The center plot includes 3 cylindrical vacuum fluence scorers which have a thickness of 1 cm and a radius of 20 cm. The bottom plot illustrates the beam characteristics of a 62.2 MeV proton beam. The initial proton beam has a cylindrical shape (radius=3 mm) and a flat intensity distribution. The energy spread is the TOPAS default value (0.757504 % of the beam energy). 1000 primary protons are simulated.

Results

Figure 5.6 shows the lateral dose distributions in one and two dimensions as well as the 1D-depth-dose-curve of the proton beam in the cylindrical water scorer at the end of the beam line.

The 1D dose profile shows a plateau starting at around 1.5 cm radial distance with a small slope to the center. The fall-off spreads over 0.5 cm. The depth-dose-curve shows a plateau with a small slope to the maximum dose spreading over approximately 2.5 cm and a fall-off spreading over 0.5 cm. For the 1D-plots the relative dose D_{rel} is given in percentage of the maximum dose deposited in the target. For the 2D-plots D_{rel} is given in percentage of the mean dose value deposited in the target area with a radius ≤ 2 cm. The statistical error is proportional to $\frac{1}{\sqrt{N}}$. In the 1D profile plot the dose is scored in bins with annuluses shapes. The bin size and the counted particle number increase as r increases. To calculate the absolute error, dose D and fluence Φ are scored in each voxel. A is the voxel surface.
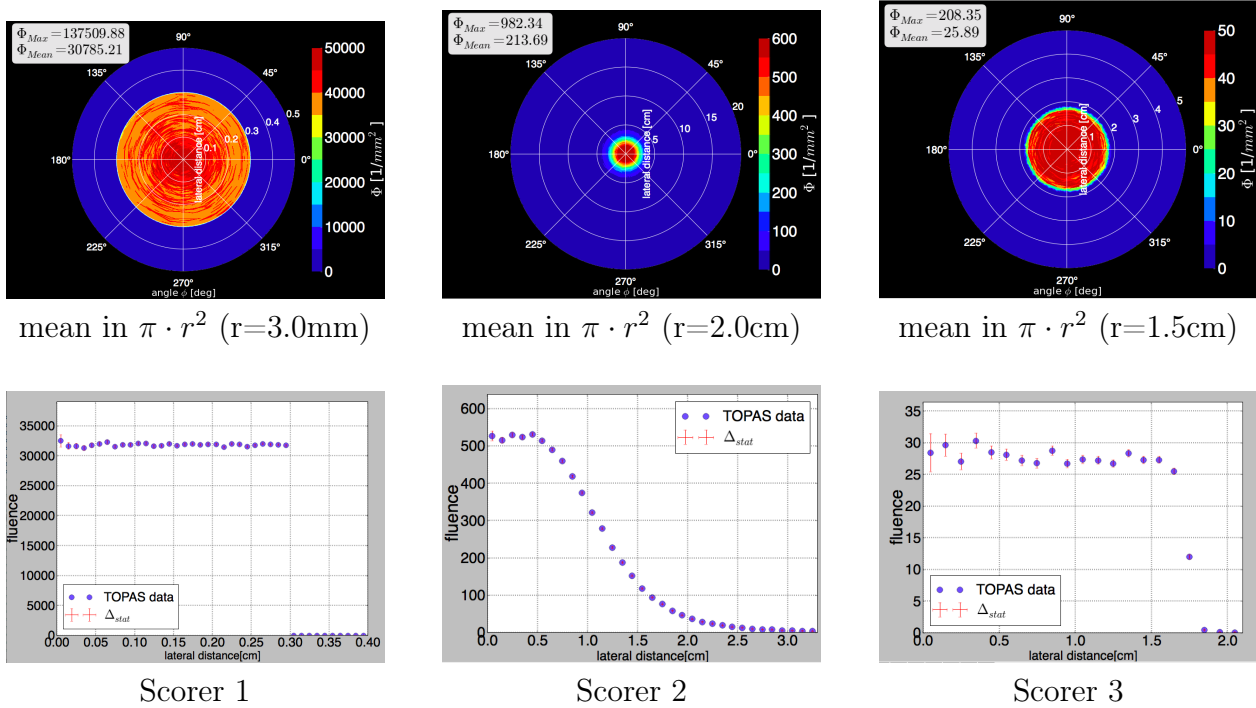
$$N = \Phi \cdot A \qquad \Delta_{stat}(\Phi) = \Phi \cdot \frac{1}{\sqrt{N}} \qquad \Delta_{stat}(D) = D \cdot \frac{1}{\sqrt{N}} \qquad (5.3)$$

The statistical error Δ_{rel} of the lateral doses is shown in the center plot. It increases as r decreases. The relative error of the maximum dose value is ≤ 7 %.
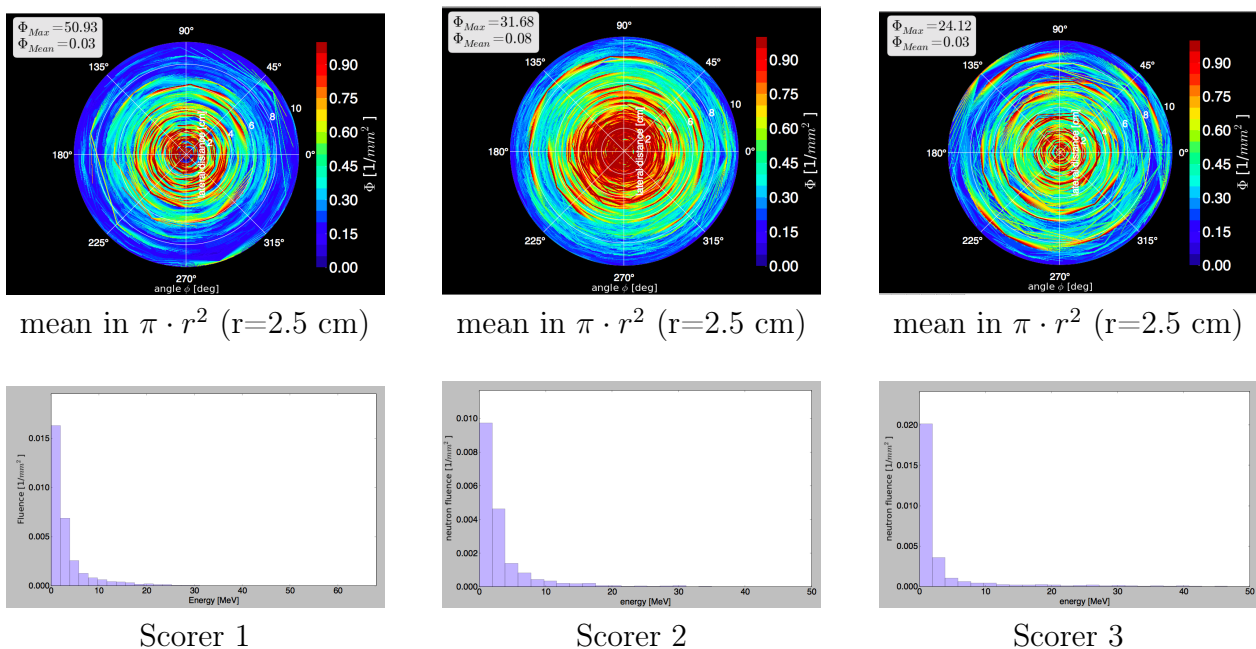
Figure 5.7 shows the 2D and 1D lateral fluence profile of the protons observed in the three red Scorers as shown in the center plot in Figure 5.5. Before traversing the beam line, the lateral beam spread of the proton beam is 0.3 cm (Scorer 1). It increases as the beam traversing the scattering system to a Gaussian like profile with a flat hat and a mean spread of approximately 2 cm (Scorer 2). Shaped by collimators the spread, which is observed in Scorer 3 has a radial width of approximately 1.5 cm corresponding to a lateral fluence profile including a flat plateau and a sharp fall-off. The fall-off spreads over 0.5 cm. The proton fluence decreases by a factor of 1000. The statistical error Δ_{rel} of the lateral fluences increases as the number of the particles, that are scored, decreases. Figure 5.8 shows 2D lateral fluences for neutrons and the corresponding energy spectra scored in the three scorers. The neutron fluences observed in Scorer 1 and Scorer 3 are more spread over the cylindrical plane compared to Scorer 2. The absolute neutron fluence loss in the beam line is 26.81 [1/mm²] and the relative fluence loss is 47.35 %. The energy spectra do not differ a lot and have a maximum at low energies. In Scorer 1 the fluence at 10 MeV has decreased to a value ≤ 10 % of the corresponding maximum value, in Scorer 2 it is ≤ 8 % and in Scorer 3 it is ≤ 10 %.
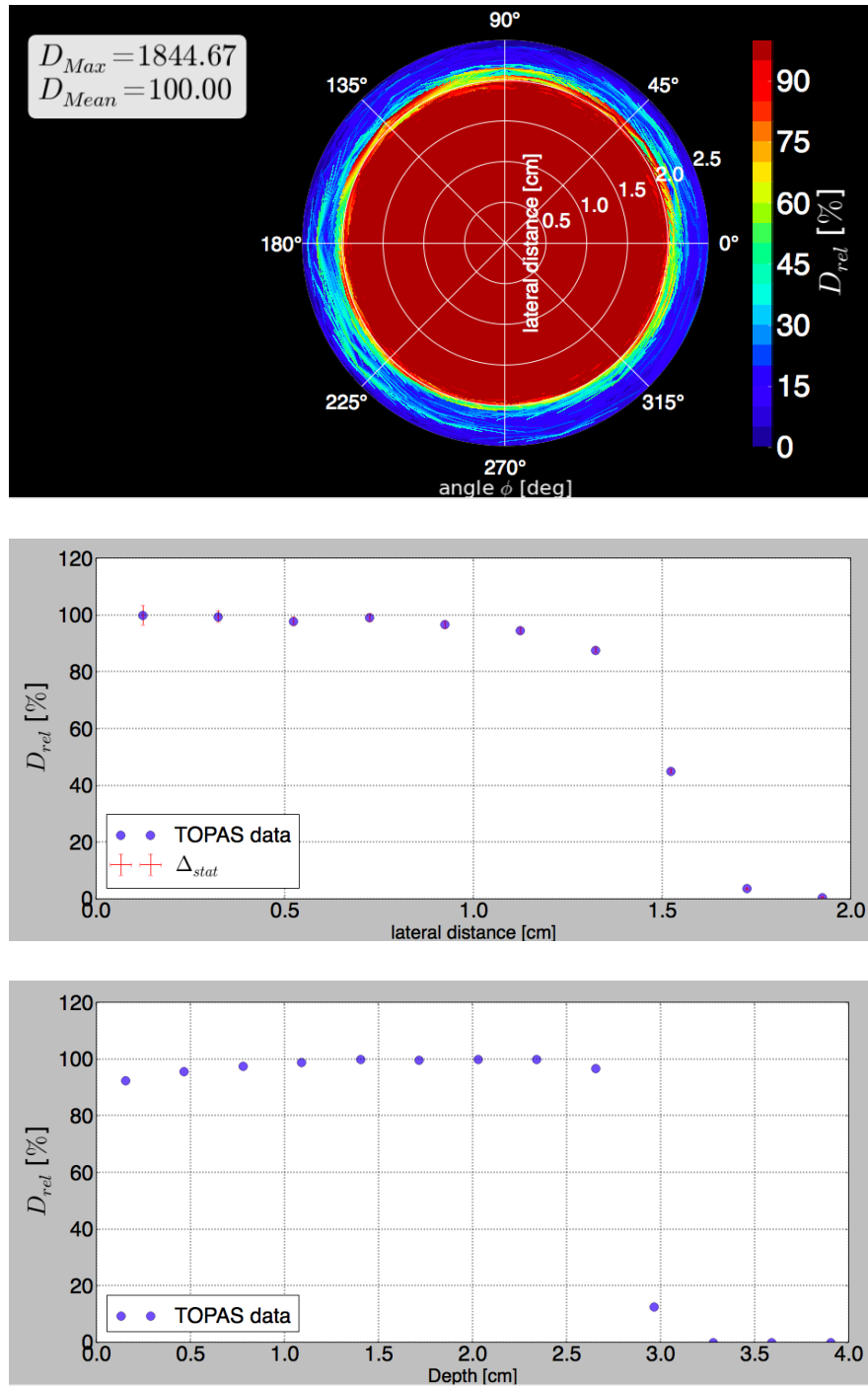
Figure 5.6: Clatterbridge lateral dose profiles and the depth-dose-curve. The simulation setting is shown in Figure 5.5. The dose is scored in the water target. The target is divided into 200 r-bins and 360 ϕ-bins for 2D lateral scorings, 10 r-bins for 1D lateral scorings and 16 z-bins for the scoring of the depth-dose-curve. $9 \cdot 10^5$ primary protons are simulated.

mean in $\pi \cdot r^2$ (r=3.0mm)   mean in $\pi \cdot r^2$ (r=2.0cm)   mean in $\pi \cdot r^2$ (r=1.5cm)

Scorer 1   Scorer 2   Scorer 3

Figure 5.7: Clatterbridge proton fluence scorings in 3 Scorers. The simulation setting is shown in Figure 5.5. 2D and 1D lateral fluences for protons are shown for the 3 red marked scorers. The mean fluence values in the 2D plots are calculated in representative circular areas. The 1D plots are not normalized. $9 \cdot 10^5$ primary protons are simulated.

mean in $\pi \cdot r^2$ (r=2.5 cm)   mean in $\pi \cdot r^2$ (r=2.5 cm)   mean in $\pi \cdot r^2$ (r=2.5 cm)

Scorer 1   Scorer 2   Scorer 3

Figure 5.8: Clatterbridge neutron fluence scorings in 3 Scorers. The simulation setting is shown in Figure 5.5. 2D lateral fluences for neutrons are shown and the corresponding energy spectra for the 3 red marked scorers. The mean fluence values in the 2D plots are calculated in representative circular areas. $9 \cdot 10^5$ primary protons are simulated.

5.3 Setup for Cell Irradiation

Construction and Simulation

To enlarge the beam for cell irradiation experiments a dual ring scattering system is used as mentioned in Figure 2.7 in the case C. The goal is to reach a flat lateral dose profile in a circle plane with 5 cm radius. The first scatterer is a 4 mm lead foil. The central disk of the second scatterer is also made of the high-Z material lead and the surrounding ring consists out of the lower-Z material aluminum. The central disk produces a Gaussian like profile, which is combined with an annulus-shaped profile from the surrounding ring. The physical thickness of the ring is constructed in the way that protons have the same energy loss as in the center disk. According to PSTAR data (aluminum: $R_0 = 22.66 \frac{\text{g}}{\text{cm}^2}$, $\rho = 2.7 \frac{\text{g}}{\text{cm}^3}$| lead: $R_0 = 35.89$ $\frac{\text{g}}{\text{cm}^2}$, $\rho = 11.43 \frac{\text{g}}{\text{cm}^3}$) the thickness of the aluminum ring has to be approximately 2.65 times bigger than the lead center disk. Taking the previous scattering studies as a role model, lateral dose distributions are scored, for different scatterer thicknesses and distances, until there were satisfying results. Figure 5.9 shows the construction plan of an optimized setting, leading to a homogeneous lateral dose profile.

A cylindrical scorer (r=9 cm, h=1 cm) is used for 1D-r lateral dose plots and the two rectangular boxes ($x1|y2$=18 cm, $y1|x2$=0.5 cm, h=1 cm) for 1D-$x|y$ dose plots. The proton beam has TOPAS defaults an an energy of 160 MeV.

Results

The upper plot in Figure 5.11 shows the 1D-r-, the center plot the 1D-x- and the lower plot the 1D-y lateral dose profiles of the setup for cell irradiation experiments for a central lead disk with a radius of 5 cm according to the construction plan shown in Figure 5.9.

The 1D-r lateral profile has a plateau with a small slope to the beam center and a sharp fall-off. The plateau spreads approximately over 5 cm and the fall-off over 1 cm. The statistical errors of the simulations of the 1D-r profile increase as r decreases. The relative error of the maximum dose value is ≤ 2.3 %. The plateau of the full length of 10 cm and the 1 cm fall-off observed in the 1D-r simulation can be observed in the 1D-$x|y$ simulations, too. As the bin size does not change the relative error stays constant to 2.22 %.

To study the dependence of the lateral profiles on the size of the lead central disk Figure 5.12 show lateral profiles for a central disk radius of 4 cm and 6 cm. The thickness of the disk stays 0.2 cm. The lateral profiles have similar shapes and Δ_{stat} values as the ones shown in Figure 5.11.
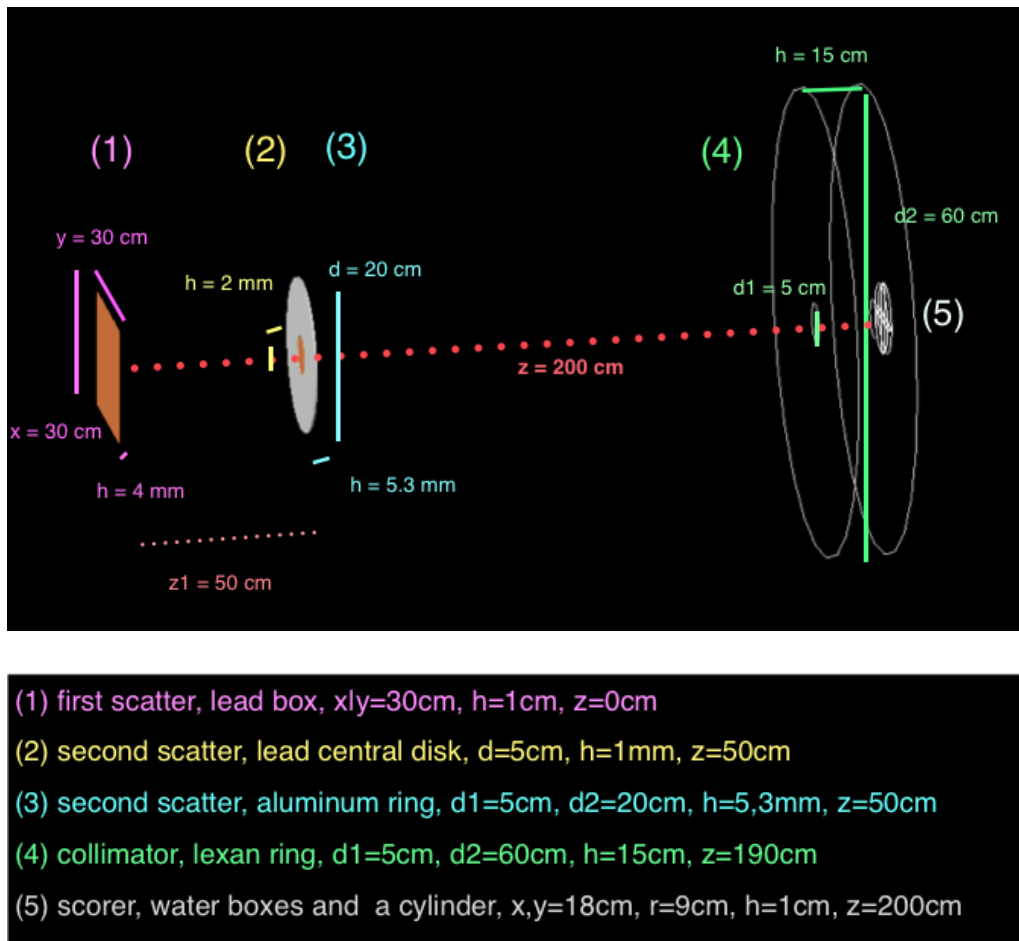
Figure 5.9: Construction plan of the cell probe setting. Description of geometries and corresponding z positions. The construction is shown for a central lead disk with a radius of 5 cm.
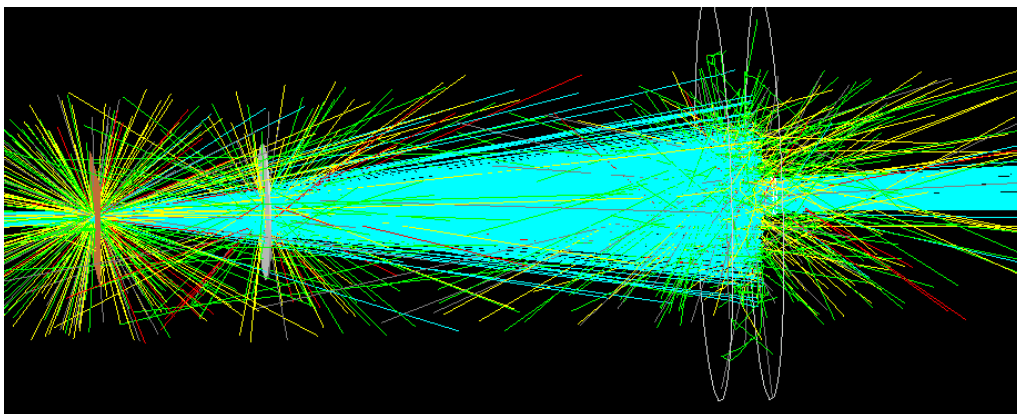
Figure 5.10: Simulation of the setup for cell irradiation experiments. The proton beam energy is 160 MeV and 1000 primary protons are simulated.
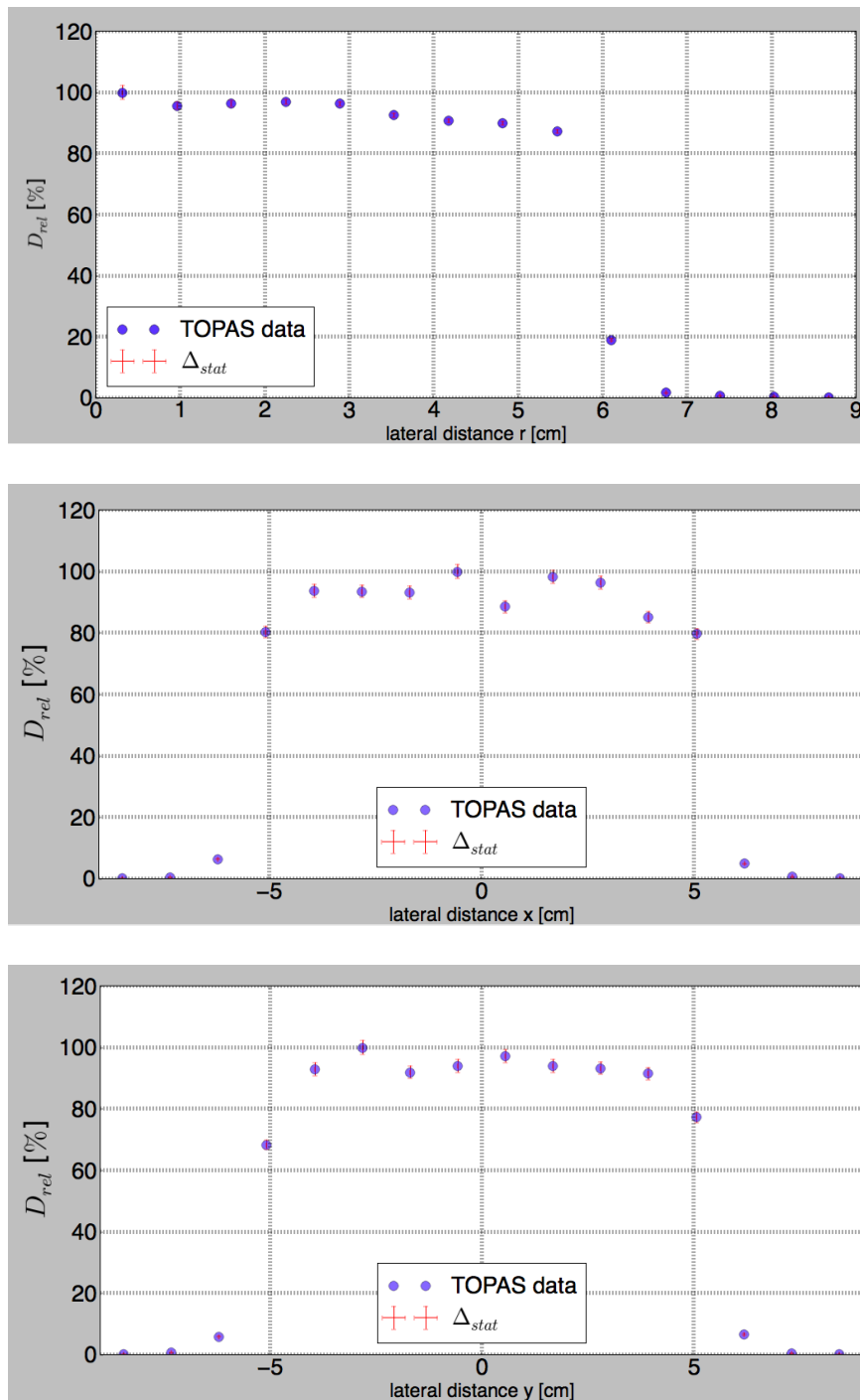
Figure 5.11: Lateral dose profiles of the setup for cell irradiation experiments with a central lead disk radius of 5 cm. The scorers are described in subsection 5.3. The simulation setting is shown in Figure 5.9. The 1D r profile is scored in 11 r bins and the 1D $x|y$ profiles in 16 $x|y$ bins. 10^6 primary protons are simulated.

central disk radius = 4 cm   central disk radius = 6 cm
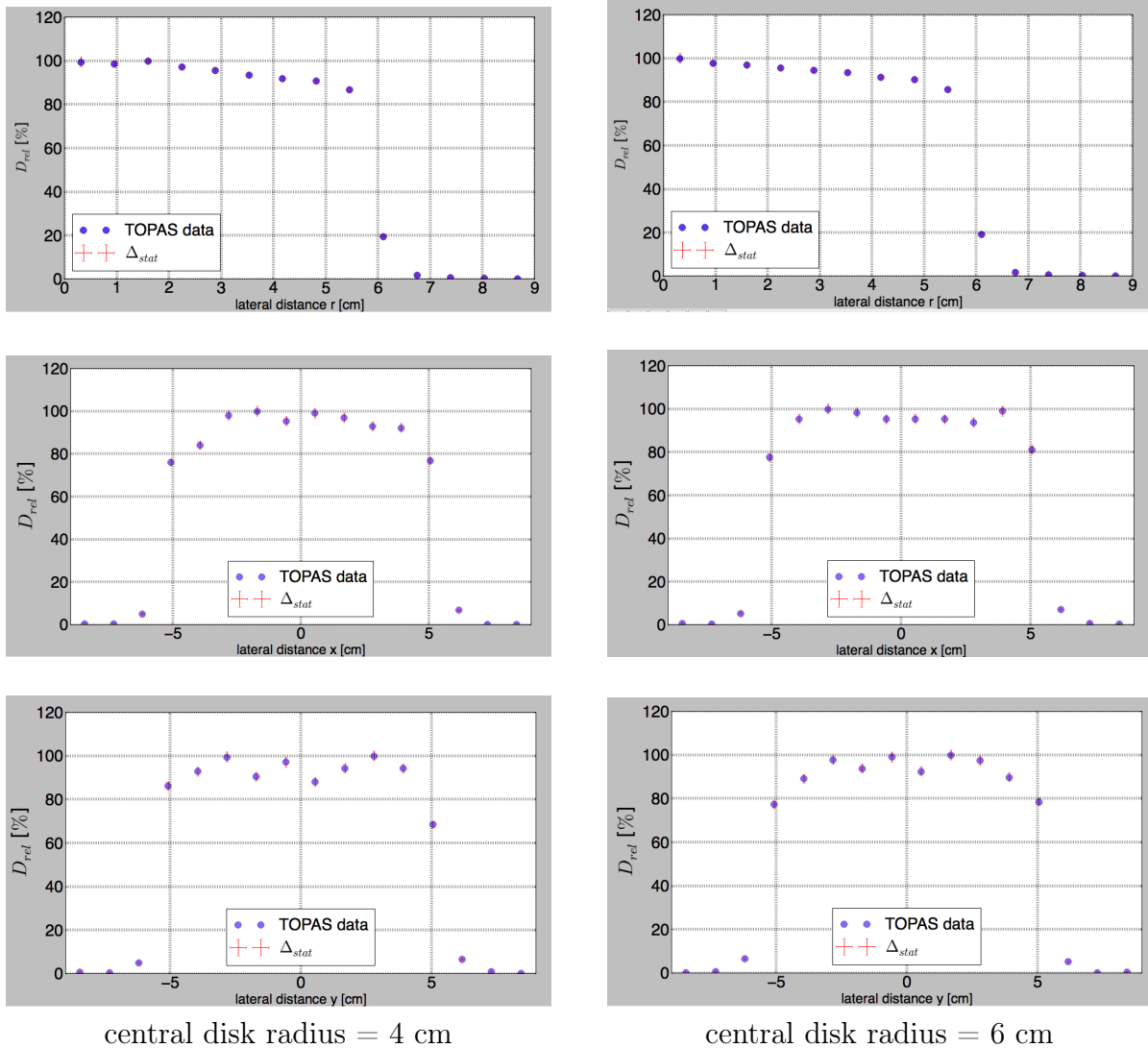
Figure 5.12: Lateral dose profiles of the setup for cell irradiation experiments with a central lead disk radius of 4 cm and 6 cm. The scorers are described in subsection 5.3. The simulation setting is shown in Figure 5.9. The 1D r profile is scored in 11 r bins and the 1D $x|y$ profiles in 16 $x|y$ bins. 10^6 primary protons are simulated.

6 IBA Gantry at Oncoray

The IBA Gantry at the Oncoray includes a scanning and a scattering mode. This chapter discusses the IBA scanning nozzle and compares simulation data with experimental measurements.

6.1 IBA Scanning Nozzle

Construction and Simulation

The IBA scanning nozzle construction data include a set of txt-files with a hierarchical order shown in Figure 6.1. The construction data are based on the IBA Gantry at Massachusetts General Hospital, which is similar to the IBA Gantry at Oncoray. The "FullSetupWithScanning.txt"-file is the starting file which loads the Gantry1 settings. The Gantry1 setting file load the Nozzle file and just the components needed for scanning. The full setup built-in TOPAS is shown in Figure 6.2.

The cylindrical scorer in the water target is 40 cm long and dose is scored in 800 z-bins. The proton beam is modulated with a step function of 10 time steps each of 1 second. 102, 100, 120, 110, 90, 94, 101, 111, 90, and 89 primary protons are simulated in 30 seconds, so each one three times.

The energy of the beam coming into the nozzle differs from the energy coming out of the nozzle. The proton beam loses energy while traversing in the nozzle through range modulation, blocking and scattering systems. To get a certain energy value of a proton beam after the nozzle the corresponding beam energy before traversing the nozzle have to be calculated. This energy can be set in TOPAS. IBA gave a polynominal equation allowing to calculate proton beam ranges before the nozzle for given beam ranges after the nozzle. Using this formula the proton beam energies before the nozzle can be calculated for the commissioning measurement energies. The calculated values are shown in Table 6.1.

Results

Figure 6.3 shows the 18 Bragg peaks simulated with TOPAS and the 18 depth-dose-curves measured at Oncoray. The detector range of 0.4 cm is already included in the measured depth-dose-curves . The TOPAS ranges are bigger than the measured ones and the simulated Bragg

Messung:	beam	energy	[MeV]			
140	145	150	155	160	165	
170	175	180	185	190	195	
200	205	210	215	220	225	226.7
TOPAS:	beam	energy	[MeV]			
141.76	146.72	151.73	156.74	161.74	166.74	
171.75	176.75	181.76	186.77	191.78	196.75	
201.77	206.76	211.75	216.75	221.71	226.69	228.38

Table 6.1: Beam energies of the Bragg peaks simulated with TOPAS and the Bragg peaks measured in the commissioning measurements.
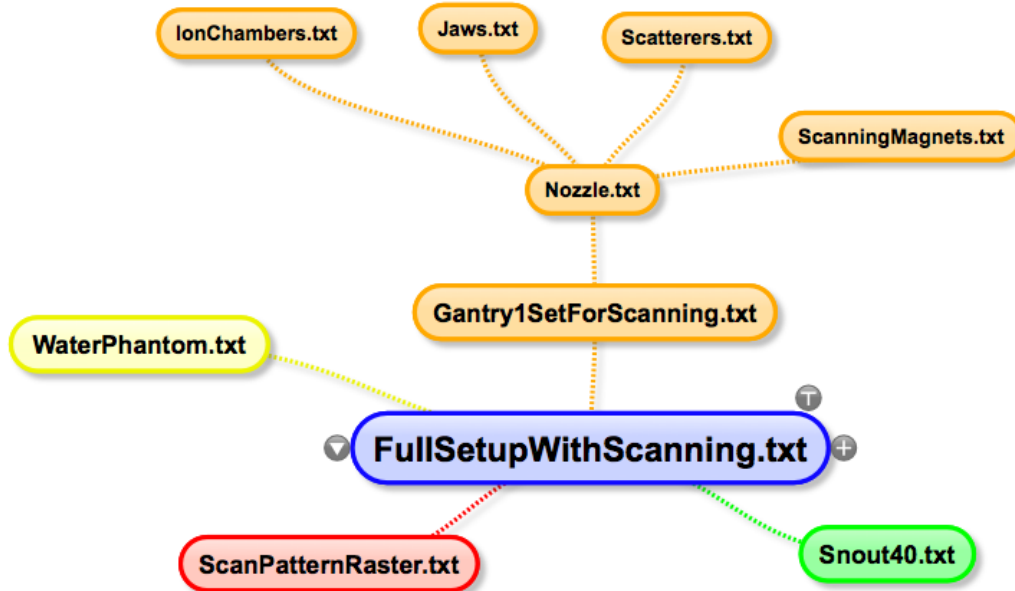
Figure 6.1: TOPAS scanning nozzle file hierarchy. Detailed information about TOPAS file structure and hierarchy can be found in the appendix (A).
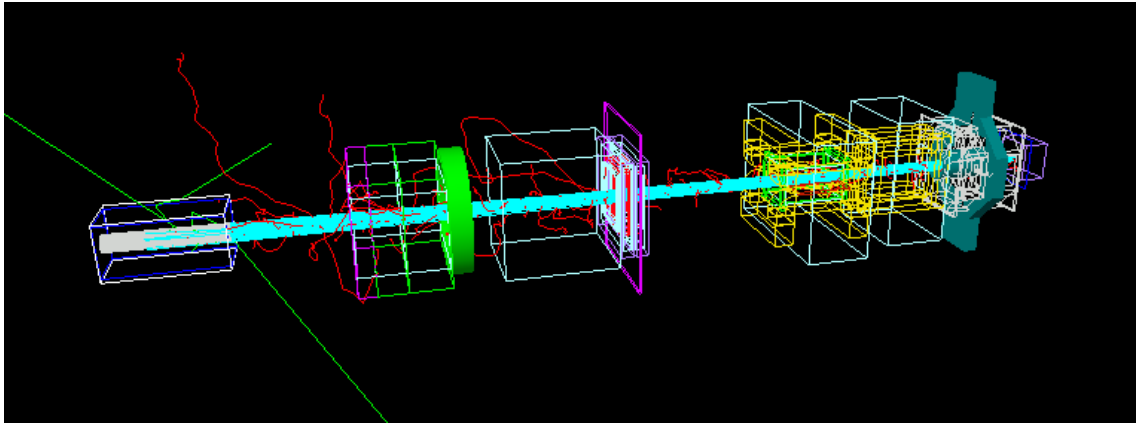
Figure 6.2: TOPAS IBA scanning nozzle. 100 primary protons are simulated.

peaks have longer tails.

Figure 6.4 shows the 140 MeV measured Bragg peak and the corresponding TOPAS one. The range analysis is done similar to Figure 4.2 by using the Python code listed in the appendix (section B.2). The commissioning measurement ranges are subtracted by the TOPAS ranges to get the range difference: $\Delta R = R_{commissioning} - R_{TOPAS}$ [cm]. The range differences for all Bragg peaks are shown in Figure 6.5 with the corresponding linear regression lines. $\Delta R_{0.9}$ and $\Delta R_{0.8}$ increases as beam energy increases, whereby the slop of the regression line of $\Delta R_{0.9}$ is higher than the one of $\Delta R_{0.8}$. The negative slope of the $\Delta R_{0.2}$ line has the highest slope modulus of the three lines. All lines intersect in a point, where the beam energy is between 140 MeV and 145 MeV.

To study, how the size of the TOPAS Bragg peak tail depends on the chosen beam energy spread, the TOPAS Bragg peaks with the beam energy of 141.76 MeV and 201.77 MeV are analyzed.

The TOPAS beam energy spread is given in percentage of the beam energy as discussed in the appendix in section A.2. The default value is 0.757504 %. The center plot in Figure 6.5 shows how the range differences of the 140 MeV proton beam behave as the beam energy spread decreases. $\Delta R_{0.2}$ decreases as beam energy spread decreases and $\Delta R_{0.9}$ increases but not as fast as $\Delta R_{0.2}$ decreases. There is a low decreasing of $\Delta R_{0.8}$ as beam energy spread shrinks. The regression lines nearly intersect in an area with a beam energy spread of around 0.6 %.
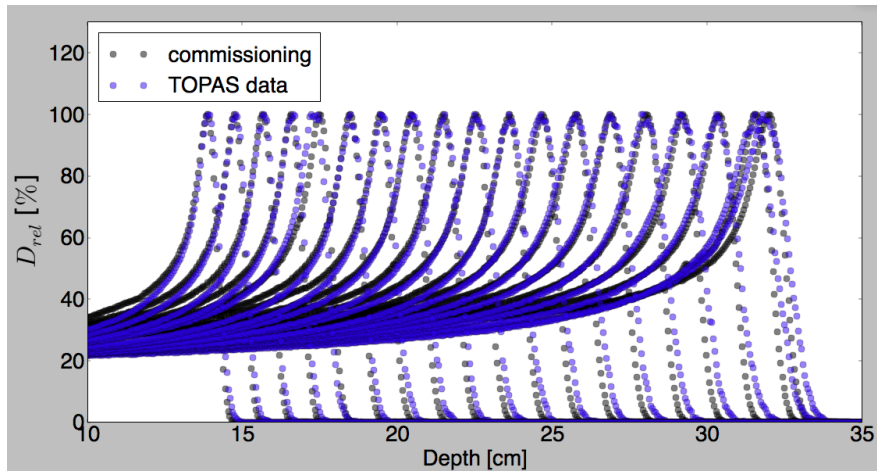
Figure 6.3: Comparison of Bragg peaks simulated with TOPAS and of Bragg peaks measured in the commissioning. The simulation setting is shown in Figure 6.2. The setting of primary proton number is explained in subsection 6.1.
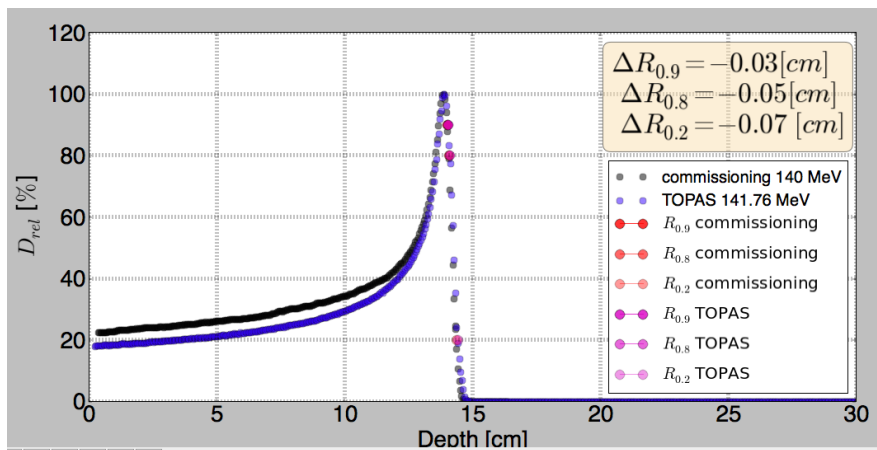
full view
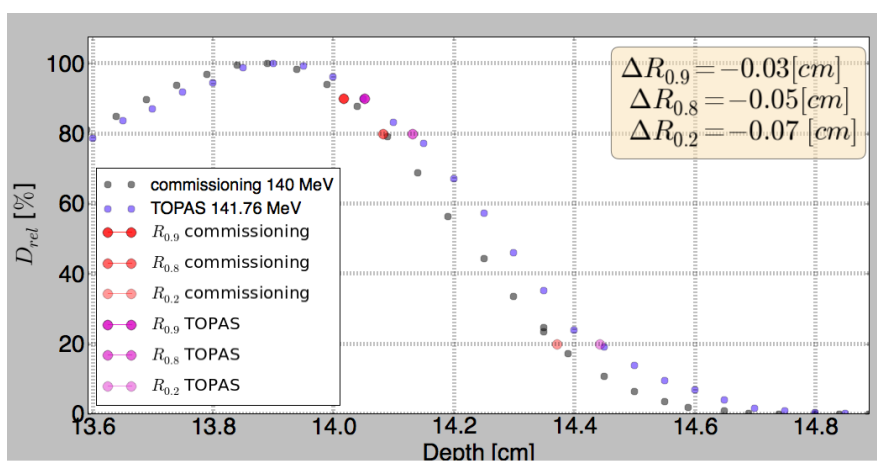
zoom view

Figure 6.4: Range difference analysis of the 140|141.76 MeV Bragg peaks. The simulation setting is shown in Figure 6.2. The setting of primary proton number is explained in subsection 6.1. The ranges are calculated by using the Python code shown in the appendix (section B.2).
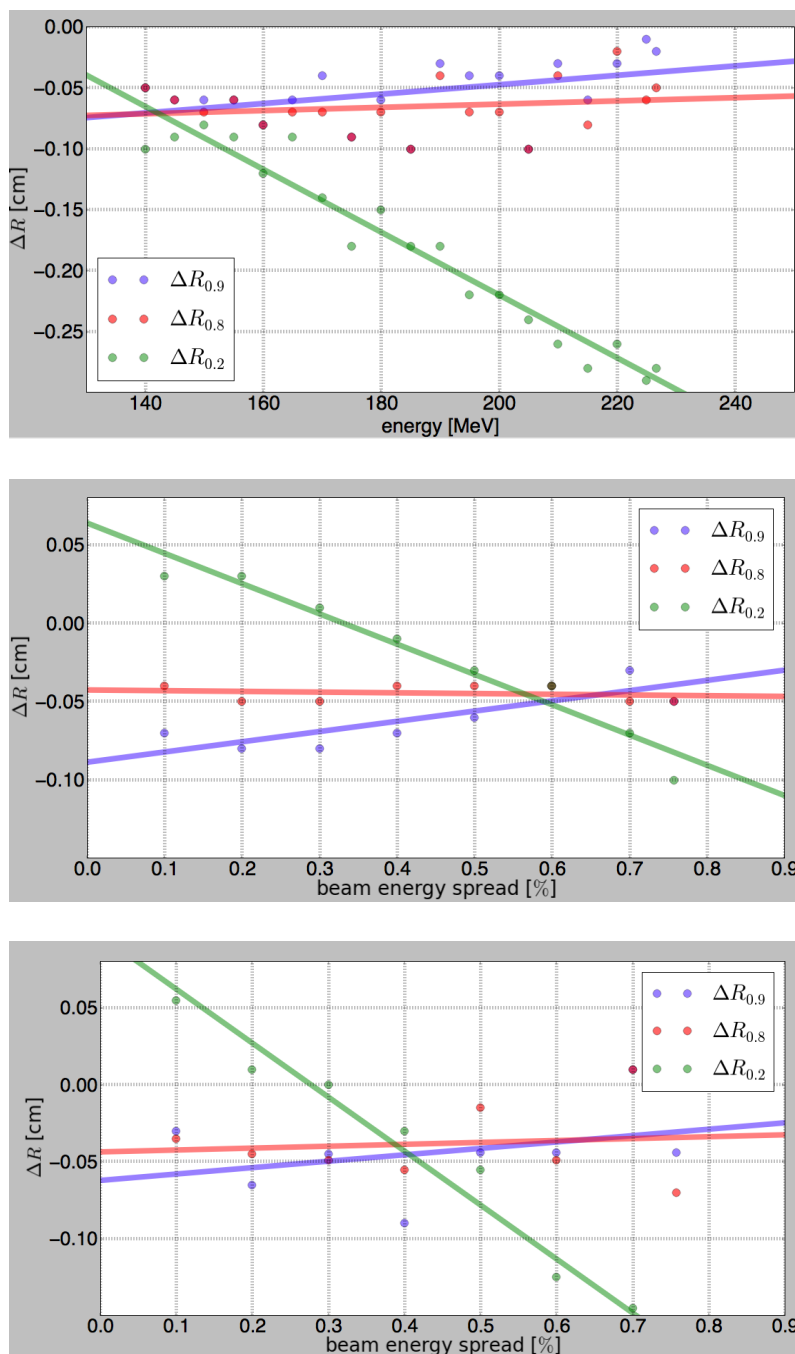
Figure 6.5: Range differences for different beam energies and beam energy spreads. The upper plot shows the range differences for all Bragg peaks shown in Figure 6.3. The center plot shows the range differences between the 141.76 MeV TOPAS beam and the 140 MeV measured one and the lower plot between the 201.77 MeV and 200 MeV Bragg peaks, when using different beam energy spreads.

7 Conclusions

7.1 Depth-Dose-Curves

1D Depth-Dose-Curves

The correct shape of the 1D-depth-dose-curves for protons at different energies and the exact ranges R_0 show that the implemented Geant4 physics modules work well for therapy energies. PSTAR uses experimental data and interpolates them with the Bethe-Bloch-Equation. As TOPAS, PSTAR uses a value of the mean excitation energy in water of I=75.0 eV, whereas Geant4 uses I=78.0 eV. TOPAS might be implemented on base of PSTAR and Figure 4.3 could be understood then as an implementation check of TOPAS. An increase of range straggling for higher energies can be observed. The longer the beam travels through the material the higher is the number of collisions leading to a larger energy spread of the particles.

The error of the simulated ranges can be decreased by increasing the binning number in combination with the number of simulated particles. The range analysis program takes the dose of the binning point which is smaller or equal to the dose value that is analyzed. Especially at the sharp fall-off of the Bragg peak the dose differences can become big and the corresponding range differences are small. For the range error calculation through binning an analytic function $D(R_0)$ is needed to determine how the dose calculation error influences the range error: $\Delta R_0 = dD/dR_0 \cdot \Delta D$.

For an exact error calculation the error has to be determined, which Geant4 made in every Monte Carlo step by solving the Boltzmann transport equation based on TOPAS default physics lists. Monte Carlo simulations make discretization and statistical errors. Discretization errors are a problem of every numerical simulation. Statistical errors are a special problem of Monte Carlo codes. Discretization and statistical errors influences each other. There are errors, because of imprecise models, too. To get an idea of such an error, different Geant4 physics lists should be compared and analyzed.

2D Depth-Dose-Distributions

The protons and the alpha particles deposit the majority of their energy at the beam stopping zone. As the ion mass increases the dose deposit in this area increases and the distal fall-off became more sharp. The lateral profile width decreases as ion mass increases, because heavier

ions move shorter distances perpendicular to the beam center after collisions with atomic nuclei. Following momentum conservation law the vertical velocity of the ion particles increases as the velocity component in beam direction decreases. The dose deposit happens almost completely through secondary electrons, which are produced by Coulomb interactions with the ions. The neutron production of the alpha particle beam is higher compared to the proton beam. Both beams can be compared, because the simulated primary proton number is four times higher than the simulated primary alpha particle number and so according to the Bethe-Bloch equation the dose deposit is equal. The increasing neutron production can be determined to the bigger geometric cross section of the alpha particles and to their fragmentation, which can be observed in TOPAS viewing mode. The dose deposit of a photon beam happens through secondary particles, which are mainly electrons. This electrons underlying a high number of Coulomb collisions, leading to smaller lateral dose spread of a photon beam compared to a proton beam.

An advantage of using protons instead of photons in therapy is the finite beam range. The larger dose deposit at the stopping region is not the main motivation of using protons, but the decreasing of the total dose deposit in the patient. However, the larger lateral spread of proton beams compared to photons is a disadvantage of proton therapy. Heavier ions decrease the total dose deposit in the patient even more and have a more sharp Bragg peak fall-off. Their disadvantage is the higher production rate of secondary particles.

7.2 SOBP

In this work spread out Bragg peaks are built by hand using either direct beam energy modulation or a range modulation wheel. For the usage of direct energy modulation the energy has to be optimized, whereas for the usage of a range modulation wheel the step angle width is the optimization parameter. The step height determines the peak distance in the spread out Bragg peak and the angle width its weight.

The larger the spread out Bragg peak has to be the more difficult it becomes to get a flat plateau by hand and the more useful it would be to have an optimization code. Such a code could be implemented by simulating Bragg peaks for the hole energy scale, which can serve as a base for any spread out Bragg peak, that has to be created. The code would always start with the deepest range and add step by step more Bragg peaks with smaller ranges and lower weights in a way making the profile as flat as possible.

The ripples of a spread out Bragg peak depending on the energy spacing. The energy spaces of 5 MeV in the right plot of Figure 4.7 are too large. 2 MeV would be better.

7.3 Scattering Systems

Single Scattering

The multiple Coulomb scattering in TOPAS corresponds to the expected single scattering behavior according to Molière's theory. The scattering angle increases as beam energy decreases and as scatter thickness increases. The lateral Gaussian profile is observed and the fitting works well for every simulated Θ_0-angle.

The Highland curve shown in Figure 2.5 is a good approximation of the experimental data from [2] including angles corresponding to relative scatterer thicknesses $d_{rel} \leq 0.01$. This leads to the conclusion, that the simulated Θ_0 angles starting to differ from Highland's formula as d_{rel} decreases are incorrect. Either the multiple Coulomb scattering physics implemented in TOPAS is wrong or the geometry setting. To exclude the second one the water scorer, which might increase Θ_0 because of multiple Coulomb scattering in the water itself, is replaced by a vacuum cylindrical fluence cross scorer with a thickness of 1 mm. No significant differences to the dose simulations in water could be observed.

The problem might be caused by the implemented TOPAS physics. A test of different physics lists would be necessary to determine if the problem is caused by the TOPAS default physics lists or by the implemented multiple Coulomb scattering physics of Geant4 in general. Geant4 uses a modified Highland-Dahl-formula, which can be studied in [4, p.51-62].

Clatterbridge Beam Line

The Clatterbridge beam line analysis results in lateral dose distributions and a depth-dose-curve, which satisfy eye cancer treatment requirements. This supports the conclusion, that the double scattering system and the range modulation wheel are correctly implemented and simulated.

There is a primary particle fluence of a factor 1000. The surface of the last fluence scorer is around 40 times larger than the surface of the first fluence scorer. So, 3-4 % of the particles entering the beam line reach the target. The flat lateral proton fluence profile becomes Gaussian through multiple Coulomb scattering after traversing the first scatterer. The stopper blocks out particles from the center, so a profile of two Gaussian is created. After the second scatterer and the range modulation wheel the beam scatters even more. The spreads of the two Gaussian increases and they melt together in the beam center leading to the homogenous fluence profile observed in Figure 5.7.

Neutrons are produced mainly by the stopper and the collimators. In the scorer before the beam line back-scattered neutrons are observed, in the other two scorers mainly the forward scattered ones. The neutron fluences and energy spectra do not differ a lot. In the scorer close to the target there are less high-energetic neutrons compared to the other two scorers. The

largest radiation damage is caused by neutrons with energies of 1 MeV.

The Clatterbridge beam line can serve as a starting point of a beam line design for cell irradiation experiments. The minimal energy, that can be produced by the cyclotron at Oncoray is 100 MeV. To use the beam line either it has to be optimized to 100 MeV or a material has to be implemented in front of the scattering system slowing down the beam to an energy of 62.2 MeV. The vacuum in the Clatterbridge scattering chamber can not be ensured at the experimental beam line at Oncoray, so the scattering properties of the beam line will change a little bit. An advantage of the Clatterbridge beam line is, that the scattering happens before the range modulation. This is useful for the construction of spread out Bragg peaks. The scattering depends on the beam energy as shown in Figure 5.3 and the system has to be adjusted when the range modulation is done before the beam is scattered.

Setup for Cell Irradiation

TOPAS gives for a double scattering system with occluding ring satisfying homogenous lateral dose distributions for cell irradiation experiments. As the radial width of the lead central disk has not much influence on the lateral dose profile its thickness can be tried to vary to observe profiles with larger plateaus. In addition, the profile shape could be improved by using occluding rings as shown in Figure 2.7 in the case D. To reduce secondary particles fluences close to the target a stopper could be implemented as shown in the Clatterbridge setting and the collimator material could be changed to brass.

Formula 2.14 can be used to calculate analytically the position z_{CS} of the second scatterer, when the position z_{FS} of the first scatterer is fixed. The slope of $\Phi(r)$ has to be minimized. Θ_{FS} and Θ_{CS} can be determined in single scattering experiments. By integrating over r the z_{CS} remains as the only unknown parameter.

$$\frac{d\Phi(r)}{dr} = 0 \rightarrow z_{CS} \tag{7.1}$$

In contrast to Clatterbridge there is no range modulation implemented in this setup. It is not needed for the first cell irradiation experiments, except the experimentalists are going to measure in the spread out Bragg peak. To obtain the scattering properties, the range modulation should be implemented after the scattering system.

7.4 IBA Gantry at Oncoray

IBA Scanning Nozzle

To optimize the IBA gantry in TOPAS the ranges and the beam energy spreads σ have to be adjusted. The upper plot in Figure 6.5 shows that the TOPAS ranges have to be decreased by approximately 0.6 mm. A first approximation of the beam energy spread is 0.5 % as it is the middle value of the two optimal σ values of the 141.77 MeV and the 201.77 MeV beam. For all energies the optimal range adjustments and σ can be calculated leading to the optimization functions $\sigma(E)$ and $E_0(E)$, whereby E_0 is the energy before the nozzle, that has to be set in TOPAS. The proceed could be adjusted for the scattering nozzle and the experimental beam line too. Further interesting tasks would be the determination of the lateral beam scattering and the scoring of the neutron fluences. CT patient plans could be in-loaded, simulated and compared with the measurements.

7.5 Résumé

TOPAS is ready for usage at Oncoray. Everything is prepared for starting a radiobiological experiment. The IBA gantry in scanning mode is adjusted.

Using this thesis and the provided TOPAS and PYTHON files the Clatterbridge beam line and the setup for cell irradiation experiments can be varied and further optimized. The IBA gantry in scattering mode can be adjusted. Detailed knowledge of Geant4 and C++ is not necessary. Through its simplicity and inner logic TOPAS is user friendly and all implemented functions have a strong focus on concrete applications needed in medical physics.

A TOPAS Software

A.1 Geometry Components

All of the geometry components must have at least the parameters as shown in Figure A.1. Also the material can be defined. World is the default parent component automatically provided with the shape of a square box, with a half widths length of 5 meter. Every component built inside a parent geometry can just be moved and rotated relative to the coordinate system of its parent.

- s:Ge/MyComponent/Parent = "World"
- s:Ge/MyComponent/Type   = "TsBox"
- d:Ge/MyComponent/TransX=0.0 cm
- d:Ge/MyComponent/TransY=0.0 cm
- d:Ge/MyComponent/TransZ=0.0 cm
- d:Ge/MyComponent/RotX=0.0 deg
- d:Ge/MyComponent/RotY=0.0 deg
- d:Ge/MyComponent/RotZ=0.0 deg

Dipole Magnet	"TsDipoleMagnet"
Quadrupole Magnet	"TsQuadrupoleMagnet"
Tabulated3DField Magnet	"TsTabulated3DField"
Range Modulator Wheel	"TsRangeModulator"
Propeller	"TsPropeller"
Ridge Filter	"TsRidgeFilter"
Multi Wire Chamber	"TsMultiWireChamber"
Aperture	"TsAperture"
Compensator	"TsCompensator"
Multi Leaf Collimator	"TsMultiLeafCollimator"
Patient in DICOM Patient	"TsDicomPatient"
Patient in XIO Format	"TsXioPatient"

Figure A.1: TOPAS default geometries. The right plot shows the default TOPAS world geometry [12, p. 22] and the right plot lists the special components built in TOPAS [12, p. 31].

The built-in TOPAS checking for volume overlap is not perfect. It works with a random set of points at each boundary. The default value of 100 can be increased in future TOPAS versions by overwriting "i:Ge/CheckOverlaps/NPoints=100". This feature is not part of the current version. Components can be assigned to parallel worlds having no physical effect. They can arbitrary overlay real mass worlds and can be ussed for scoring for example. Every geometry component can be marked with a color and a special drawing style like "Solid", "Wireframe" or "Fullwireframe".

There are three dividable geometry components: TsBox (XBins, YBins, ZBins), TsCylinder (RBins, PhiBins, ZBins) and TsSphere (RBins, PhiBins, ThetaBins) and also all generic Geant4 components [5]. When a component is marked with the type="Group", than it is no actual solid, but can serve as a parent. By moving a group all components built-in will move the same way. There are 12 special components as shown in Figure A.1.

A.2 Particle Sources and Physics

Beam Sources/Beam Position

TOPAS allows any number of particle sources with no limitation on how they can be mixed. The source position needs always an acccociated geometry component. In TOPAS all geometry information reside in the components. The default parameters for beam source and beam position are shown in Figure A.2. The beam energy spread is given as the percentage of the mean energy. All three beam types can be shaped in more detail in their spatial and energy distributions (Figure A.2). It is possible to filter the sources by charge, atomic mass, kinetic energy, momentum and name. Filters can be combined. Geant4 generic ions can by integrated with "GenericIon(6,10)", whereby the first number is the atomic number and the second is the mass number. Ions of atomic number less than 3 require a definition by name like "deuteron", "triton", "He3" or alpha.

- s:So/Default/Type = "Beam"
    # Beam, Twiss, PhaseSpace,
    GeneralParticleSource or Seed
- s:So/Default/Component = "BeamPosition"
- s:So/Default/BeamParticle = "proton"
- d:So/Default/BeamEnergy = 169.23 MeV
- d:So/Default/BeamEnergySpread = 0.757504
    unitless
- s:So/Default/BeamShape = "Ellipse"
    # Point, Ellipse or Rectangle
- i:So/Default/NumberOfHistoriesInRun = 0

- s:Ge/BeamPosition/Parent="World"
- s:Ge/BeamPosition/Type="Group"
- d:Ge/BeamPosition/TransX=0. m
- d:Ge/BeamPosition/TransY=0. m
- d:Ge/BeamPosition/TransZ= Ge/World/HLZ m
- d:Ge/BeamPosition/RotX=180. deg
- d:Ge/BeamPosition/RotY=0. deg
- d:Ge/BeamPosition/RotZ=0. deg

- d:So/Default/BeamHWX = 10. cm # extent of
    ellipse or rectangle shape in the X direction
- d:So/Default/BeamHWY = 10. cm $ extent of
    ellipse or rectangle shape in the Y direction
- d:So/Default/BeamAngularSpreadX = 0.0032 rad
- d:So/Default/BeamAngularSpreadY = 0.0032 rad
- s:So/Default/BeamXYDistribution = "Gaussian"
    # Flat or Gaussian
- d:So/Default/BeamStandardDeviationX = 0.65 cm
    # distribution used for Gaussian
- d:So/Default/BeamStandardDeviationY = 0.65 cm
    # distribution used for Gaussian

- s:Ph/ListName = "Default"
- s:Ph/Default/Type= "Geant4_Modular"
- sv:Ph/Default/Modules = 6 "g4em-standard_opt3"
    "g4h-phy_QGSP_BIC_HP" "g4decay"
    "g4ion-binarycascade" "g4h-elastic_HP"
    "g4q-stopping"
- d:Ph/Default/EMRangeMin = 100. eV
- d:Ph/Default/EMRangeMax = 500. MeV
- i:Ph/Default/dEdXBins = 220
- i:Ph/Default/LamdaBins = 220

Figure A.2: TOPAS defaults for the beam source (upper left), the beam position (upper right), the beam shape (lower left) and the physics list (lower right) [12, p. 62-67].

Physics List

Like Geant4 the underlying physics interactions in TOPAS are set in "Physics List", which specify what particles and physics processes are defined, plus various cuts and options. The default list (Figure A.2) has been worked out well for proton therapy at Massachusetts General

Hospital [6] and includes models for protons, neutrons, helium ions, deuterons, tritons, photons, electrons, etc. It is possible to set range cuts for all particles and turn on fluorescence. The related TOPAS module names for the Geant4 class names are listed in the TOPAS user guide [12, p. 68-70]. There are pre-made, complete lists in Geant4 called reference physics list. They do not support parallel worlds so scoring with a different set of divisions for a dividable component will not be allowed. Physics control in a specific component can be achieved by "d:Ge/World/Max StepSize = 100". There is the possibility to set up own physics lists in Geant4 and integrate them in TOPAS.

A.3 Scoring

Scoring in a volume and at a surface are the two basic scorer classes in TOPAS. A scorer definition is done by: "s:Sc/MyScorer/Quantity = "DoseToMedium". It is possible to build own scorers.

Scoring Quantities

Quantities for volume scorers are: DoseToMedium (sum of energy deposits divided by mass), DoseToWater (energy-dependent stopping power conversion), DoseToWaterBinned (about 50 % faster, but less accuracy than DoseToWater), DoseToMaterial, EnergyDeposit, Fluence (from sum of step lengths divided by volume), EnergyFluence, Charge, EffectiveCharge, StepCount, LETDDeposit (dose-averaged LET, energy divided by step length) and LETDEnergyDeposit. To get LET you have to divide LETDeposit through LETDEnergyDeposit. For neutral particles the stopping power is taken from proton stopping power for a fixed energy like: "Sc/MyScorer/SubstituteEnergyForNeutralScaling (default = 100 MeV)". The DoseToWaterBinnend scorer can be optimized by Proton- and ElectronEnergyBinSizes and Min/Max - energies for stopping power ratios settings. For Charge and EffectiveCharge scorers if a particle reaches zero energy in the scoring volume, charge is accumulated, and if a particle is generated in the scoring volume, charge is subtracted. Surface scorer quantities are "SurfaceCurrent", "SurfaceTrackCount" and "PhaseSpace".

A surface scorer must indicate the component and surface name like: "s:Sc/MyScorer/Surface = "Phantom/ZMinusSurface". In a TsBox or G4Box specific surfaces can be "X(YZ) Minus(Plus) Surface". In a TsCylinder/G4Tube the specific surfaces are "ZMinus(Plus)Surface", Minus(Plus) PhiSurface and "Inner(Outer)CurvedSurface". In a TsSphere/G4Sphere there are "Inner (Outer) CurvedSurface and "Minus(Plus) Phi(Theta) Surface" [12, p. 72-74].

PhaseSpace

PhaseSpace refers to the technique of saving and replaying a set of particles at a given surface. The positions, particle types and momenta of a given particle number will be saved and are used as short values for simulations. TOPAS follows the IAEA Phase Space Standard described at http://www-nds.iaea.org/phsp and also allows generation of a Binary or ASCII phase space like: "s:Sc:/MyScorer/OutputType = "IAEA_ASCII(Binary)"". The advantage of a Binary format is that it is compact and hence suitable for large files, where the advantage of ASCII is that it is a human-readable text. At least ten columns of data are provided: "X(YZ) position, U,V (direction cosine of momentum with respect to X,Y), energy in MeV, weight, particle ID (1=photon, 2=electron, 3=positron, 4=neutron, 5=proton), flag to indicate the sign of the third direction cosine and a flag to indicate whether this is a new history". The positions are relative to the center of the world. It is possible to include additional columns to PhaseSpaceOutput like TimeOfFlight, RunID, EventID, etc [12, p. 74-75].

Filtering Scorers

Limiting the scoring quantities can be realized through filtering by particle generation ("Primary/ Secondary"), charge ("Positive/Negative/Neutral"), atomic mass, particle's initial kinetic energy and momentum, kinetic energy and momentum of particle or its ancestor when it hit the scoring component. It can also be filtered by the process that created particle or any ancestor ("hIoni", "eBrem"), particle/ancestors name, particle/ancestors origin volume and by whether particle/ancestors interact or transverse in a volume. Filtering whether a particle goes in or out of a scoring surface is allowed. TOPAS can filter on DICOM RT structure sets and any filter property can be set by time features to produce time-depending filtering [12, p. 76-79].

Output/Splitting/Statistics

The TOPAS scoring data can be written into files by setting file name and type. With "s/MyScorer/OutputFile = "myOutputFileName" an output file name is specified and with "s/MyScorer/OutputType = "csv"("binary", "Root", "Xml", "DICOM") the appropriate output type can be set. For scoring in the dividable components: TsBox, TsCylinder and TsSphere it is possible to score in every bin. Also a scorer can be binned by incident particle/ancestors energy, when it first hits the scoring component by defining the number of EBins and EBin maximum and minimum. Any scorer can be binned by the time of the hit with the definition of bin number, minimum and maximum time. Splitting a scorer into separate scorers depending on the current value of any selected time feature can be realized with "s:Sc/MyScorer/SplitByTimeFeature = some_time_feature_name". If the time feature is a step function, one split scorer is made for every time feature value, if time feature is a continu-

ous function it's necessary to add the command line: "dv:Sc/MyScorer/SplitByTimeFeature = 5 0. 90. 180. 270. 360. deg". Statistical informations of the scored histories can be generated with the Report-command like: "s:Sc/MyScorer/Report = "Sum" (One or more Sum, Mean, Histories, Count_In_Bin, Second_Moment, Variance, Standard_Deviation, Min_Max)". Turning a scorer off can be arranged by using: "s:Sc/MyScorer/Active = "False" ("True")". [12, p. 80-84] Variance reduction which is still under development in TOPAS, should always be double checked by an equivalent setup without variance reduction by the user. It is highly depending on specific geometry and is further described for TOPAS in [13].

A.4 Graphics, Time Feature and Overall Control

Graphics

Colors in TOPAS are defined through their red, green and blue components like "iv:Gr/Color/ ligthblue = 3 175 255 255". Different types of graphics can be added at the same time: "s:Gr/MyGraphic1/ Type = "OpenGL" (HepRap, VRML, DAWN, RayTracerX)". Also an external filename can be added with "s:Gr/Graphic1/FileName = "MyFileName"". The user can choose, whether he includes geometry, trajectories and step points which are by default included. Also axes can be included in a chosen component with a specified size. Graphics can be refreshed after every history, every run or session and like a scorer visualization can be deactivated. Extra options like zooming, setting view angles, moving and increasing the viewing window or saving views as eps file (b:Gr/MyGraphic1/CopyOpenGLToEPS = "True") are included in TOPAS. Trajectory coloring can be done by charge, particle type, origin component, energy, momentum, generation or creator process. The default value is charge (s:Gr/MyGraphic1/ColorBy = "Charge"). The default color values for "ParticleType" are similar to the Geant4 defaults (gamma = green, e^- = red, e^+ = blue, $\pi^{\pm}$ = magenta, proton = cyan, neutron = yellow, other = grey). For ColorBy = "OrginVolume" trajectories are grey unless they come from the marked volume. To filter which trajectories will be in the graphics, similar syntax can be used as in filtering scorers. Visualization control of a specific component can be done by setting a new component parameter like "s:Ge/MyComponent/Color = "red"".

Time Feature

The definition of time-depending behavior like motion, beam current modulation or starting and stopping of scoring activities is realized by the TOPAS time feature through a set of parameters describing the change of a time feature value. The user provides parameters that define the time function, like a linear change, and TOPAS creates a parameter value for this function and continually updates this parameter. Figure A.3 shows examples how continuous and step time functions can be used. Step functions just cycle back and do not need a repetition

interval like the continuous functions. They also can control boolean values, which activates or deactivates a scorer for example. In addition to specifying time features you need to specify an overall time sequence [12, p. 92-94].

```
• s:Tf/ArmRot/Function = "Linear deg"
• d:Tf/ArmRot/Rate = 2. deg/ms
• d:Tf/ArmRot/StartValue = 0.0 deg
• d:Tf/ArmRot/RepetitionInterval = 50. ms
• d:Ge/Arm/RotX = 0. deg + Tf/ArmRot/Value
    # affected component position
```

```
• s:Tf/ScoringOnOff/Function="Step"
• dv:Tf/ScoringOnOff/Times =10 10
    20 30 40 50 60 70 80 90 100 ms
• bv:Tf/ScoringOnOff/Values=10 "true"
    "false" "true" "false" "false"
    "true" "true" "true" "false" "true"
```

```
• s:Tf/ImageName/Function = "Step"
• dv:Tf/ImageName/Times = 3 10 20 30 ms
• sv:Tf/ImageName/Values = 3 "lung-1"
    "lung-2" "lung-3"
o The first value is used for times
    0 to 10 ms.
o The second value is used for times
    10 to 20 ms.
o The third value is used for times
    20 to 30 ms.
o After 30 ms, the value cycles back
    to the first value.
```

```
• s:Tf/BeamCurrent/Function="Step"
• dv:Tf/BeamCurrent/Times = 1 10 ms
• iv:Tf/BeamCurrent/Values = 1 10
• s:Tf/BeamWeight/Function="Step"
• dv:Tf/BeamWeight/Times =10 1 2 3
    4 5 6 7 8 9 10 ms
• iv:Tf/BeamWeight/Values =10 1 1
    1 2 2 2 2 4 4 4
• i:Tf/BCM/Value = Tf/BeamWeight/Value
    * Tf/BeamCurrent/Value
• So/Default/NumberOfHistoriesInRun
    = Tf/BCMValue
```

Figure A.3: TOPAS time feature examples [12, p. 92-93]. The upper left plot shows a continuous linear function controlling the position of a component. The upper right plot shows a step function controlling a boolean value, and the lower left plot one, that controls a string value. The lower left plot shows how two time functions can be combined.

Overall Control

There are three time modes in TOPAS. The fixed time mode, the sequential time mode and the random time mode. In fixed time mode TOPAS will run with no time variation, just number of histories in run has to be defined (i:So/Default/NumberOf HistoriesInRun = 100). If there are time features in the file they will all be evaluated with time equals zero. Changing this time works with "d:Tf/TimlineStart = 10. s". For more than one source TOPAS will run until all sources have run all their histories. To run several runs at fixed time intervals the sequential time mode has to be used, where you have to define TimelineStart, TimelineEnd and NumberOfSequentialTimes. At each interval the source will run the indicated number of histories. Printing time feature information to a log-file and the console works with: "i:Tf/Verbosity = 2 (default 0, 1 log-file, 2 get update messages)". To implement beam current modulation it is possible that NumberOfHistoriesInRun get its value from a time feature. The random time mode generates histories per run, with a randomly

sampled time at each run. With this mode you can study features that do not appear on sequential time mode and do statistics at lower run.

To use the random mode you have to specify start and end time, turn on RandomizeTimeDistribution by setting it "True", and set the source's NumberOfHistoriesInRunJob (for example = 1000). For each history a random time between start and end time will be sampled. To implement beam current modulation the source needs a time-dependent ProbabilityOfUsingAGivenRandomTime (Default = Tf/MyBCMTimeFeature/Value). If TOPAS should pause for interactive Geant4 commands the command will be: "s:Ts/PauseForGeant4Commands = "Never" (or one or more of "BeforeInit", "BeforeSequence" or "BeforeQuit")". Additional overall parameters are: Seed (i:Ts/Seed = 1 starts a random seed), setting how often history count should be printed on console (i:Ts/ShowHistoryCountAtInterval = 1), making count reuse a single line of console (b:Ts/ShowHistoryCountOnSingleLine = "False"), dump a full list of parameters to file TopasParameterDump.html (b:Ts/DumpParameters = "True") or increasing details of tracking (i:Ts/TrackingVerbosity = 0, larger integer for more detail) [12, p. 95-96].

A.5 Extending TOPAS

For additional functionality TOPAS can be extended by writing new geometry components, scorers, filters or physics list through new C++ classes, which can be linked into the rest of TOPAS with "topas/ extensions/TsExtensionsManager.cc" and than by relinking TOPAS. The TOPAS parameter system can be used to provide parameters to your classes. TOPAS geometry components are like small pieces of Geant4 detector construction class [5]. The added geometry component will be a concrete implementation of the base class: TsVGeometryComponent. Scorers must be written carefully to avoid slowing down the simulation. Scorer's ProcessHits method is called for every hit in the scoring component and slow operations such as string comparisons should be avoided during this method. The code should be written that way that these slow operation occur only during construction, saving values and pointers in class variables and use these pre-calculated values in the ProcessHitMethod. At a minimum a scorer should have a constructer, a destructor and a ProcessHitMethod. Also by constructing a filter slow operations like ResolveParameters method or CacheGeometryPointers method should only be performed during the constructor. Adding own physics lists is possible, but requires a substantial Geant4 expertise, so it is recommended to start with a reference physics list. A further description of extending TOPAS you can find elsewhere [12, p. 102-107].

B Example Files

B.1 TOPAS Example File

```
# Program to define a cylinder water phantom and corresponding scorer to get
# data for a 1D  Depth-Dose-Curve. The 140 MeV proton beam has TOPAS default
# paramaters, which are given and commented as well.

##########################################################################
# World
##########################################################################
# The default TOPAS world parameters are overwritten. The world is that as
# invisible and won't appear in the viewing mode.

d:Ge/World/HLX=30.0 cm                      # half lengths
d:Ge/World/HLY=30.0 cm
d:Ge/World/HLZ=100.0 cm
s:Ge/World/Material="Vacuum"                # TOPAS vacuum definition
b:Ge/World/Invisible = "TRUE"               # invisible in the viewing mode


##########################################################################
# Geometry
##########################################################################
# TsCylinder and and TsBox are placed into the world. Geometric properties,
# position in the world, material, color and drawing style are defined.

# Cylinder1
s:Ge/Cylinder1/Parent="World"              # component placed in the world
s:Ge/Cylinder1/Type="TsCylinder"           # TOPAS dividable component
d:Ge/Cylinder1/RMin=0.0 cm                 # geometry parameters
d:Ge/Cylinder1/RMax=10.0 cm
d:Ge/Cylinder1/SPhi=0.0 deg
d:Ge/Cylinder1/DPhi= 360. deg
d:Ge/Cylinder1/HL=10. cm                   # half cylinder length
s:Ge/Cylinder1/Material="water"            # TOPAS water definition (I=75eV)
d:Ge/Cylinder1/TransX=0. cm                # relative position in the world
d:Ge/Cylinder1/TransY=0. cm
d:Ge/Cylinder1/TransZ=0. cm
d:Ge/Cylinder1/RotX=0.0 deg
d:Ge/Cylinder1/RotY=0.0 deg
d:Ge/Cylinder1/RotZ=0.0 deg
s:Ge/Cylinder1/Color="white"                   # adding color
s:Ge/Cylinder1/DrawingStyle = "Wireframe"      # adding drawing style
```

```
# Box1
s:Ge/Box1/Parent="World"                    # TOPAS water box
s:Ge/Box1/Type="TsBox"
d:Ge/Box1/HLX=10.0 cm
d:Ge/Box1/HLY=10.0 cm
d:Ge/Box1/HLZ=10.0 cm
s:Ge/Box1/Material="Water"
d:Ge/Box1/TransX=0. cm
d:Ge/Box1/TransY=0. cm
d:Ge/Box1/TransZ=0. cm
d:Ge/Box1/RotX=0.0 deg
d:Ge/Box1/RotY=0.0 deg
d:Ge/Box1/RotZ=0.0 deg
s:Ge/Box1/Color="white"
s:Ge/Box1/DrawingStyle = "Wireframe"
b:Ge/Box1/Invisible = "True"                # hiding the box




########################################################################
# Scorer
########################################################################
# Two scorers are built, one for the cylinder and one for the box. Scorer1
# scores dose in 200 z-bins for 1D Depth-Dose-Curves. Scorer2 scores at 200
# x- and y-bins dose in Box1 for 2D Depth-Dose-Curves.

# Scorer1 DosetoMedium
s:Sc/Scorer1/Quantity = "DoseToMedium"           # Fluence, EnergyFluence, ...
s:Sc/Scorer1/Component = "Cylinder1"             # scoring component
b:Sc/Scorer1/OutputToConsole = "TRUE"            # shows scorings at the shell
s:Sc/Scorer1/OutputFile = "Data-Cylinder1"       # name of output file
s:Sc/Scorer1/OutputType = "csv"                  # type of output file
s:Sc/Scorer1/IfOutputFileAlreadyExists = "Overwrite"
# also "Increment" possible to create a new output file
i:Sc/Scorer1/RBins = 1
i:Sc/Scorer1/PhiBins = 1
i:Sc/Scorer1/ZBins = 1                            # 1bin = 1mm

# Scorer2 DosetoMedium
s:Sc/Scorer2/Quantity = "DoseToMedium"
s:Sc/Scorer2/Component = "Box1"
b:Sc/Scorer2/OutputToConsole = "TRUE"
s:Sc/Scorer2/OutputFile = "Data-Box1"
s:Sc/Scorer2/OutputType = "csv"
s:Sc/Scorer2/IfOutputFileAlreadyExists = "Overwrite"
i:Sc/Scorer2/XBins = 1                            # 1bin = 1mm
i:Sc/Scorer2/YBins = 1
i:Sc/Scorer2/ZBins = 1

# Deactive a scorer or scoring just neutrons can be arranged through the
# following settings
# b:Sc/Scorer2/Active = "False"
# sv:Sc/Scorer2/OnlyIncludeParticlesCharged = 1 "Neutral"
# i:Sc/Scorer2/OnlyIncludeParticlesOfAtomicMass = 1
```

```
##############################################################################
# Particle Source and Beam Position
##############################################################################
# Following parameters are TOPAS defaults, except energy is overwritten. These
# defaults are discussed in subsection 3.4.

# Particle Source
s:So/default/Type = "Beam"                          # also Phasespace, Twiss
s:So/default/Component = "BeamPosition"             # beam origin component
s:So/default/BeamParticle = "proton"                # neutron, e-, gamma, alpha,...
d:So/default/BeamEnergy = 140.00 MeV                # beam energy
s:So/default/Beamshape = "Ellipse"
u:So/default/BeamEnergySpread = 0.757504            # energy spectrum shape
d:So/default/BeamHWX=10 cm
d:So/default/BeamHWY=10 cm
d:So/default/BeamAngularSpreadX=0.0032 rad
d:So/default/BeamAngularSpreadY=0.0032 rad
s:So/default/BeamXYDistribution = "Gaussian"
d:So/default/BeamStandardDeviationX=0.65 cm
d:So/default/BeamStandardDeviationY=0.65 cm


#Beam Position
s:Ge/BeamPosition/Parent="World"
s:Ge/BeamPosition/Type="Group"
d:Ge/BeamPosition/TransX=0. m
d:Ge/BeamPosition/TransY=0. m
d:Ge/BeamPosition/TransZ= -30 cm                    # beam start point shift
d:Ge/BeamPosition/RotX=0. deg
d:Ge/BeamPosition/RotY=0. deg
d:Ge/BeamPosition/RotZ=0. deg



##############################################################################
# Overall Control
##############################################################################


i:So/default/NumberOfHistoriesInRun = 100
# number of simulated particles
Ts/PauseForGeant4Commands="BeforeQuit"
# viewing mode don't quit after last history is simulated
```

```
#########################################################################
# View
#########################################################################

s:Gr/ViewA/Type = "OpenGL"                      # opens viewing mode
i:Gr/ViewA/WindowSizeX = 1200
i:Gr/ViewA/WindowSizeY = 650
d:Gr/ViewA/Theta = 30 deg                       # circle coordinates
d:Gr/ViewA/Phi = 20 deg
u:Gr/ViewA/Zoom = 1.                            # zoom function, 1 is no zoom
u:Gr/ViewA/TransX = 0.0                         # moves whole window
u:Gr/ViewA/TransY = 0.0
s:Gr/ViewA/Projection = "Perspective"          # special viewing perspective
d:Gr/ViewA/PerspectiveAngle = 30 deg
b:Gr/ViewA/CopyOpenGLToEPS = "False"           # creates EPS -file
b:Gr/ViewA/IncludeAxes = "true"                # coordinate axes
d:Gr/ViewA/AxesSize = 0.1 m
s:Gr/ViewA/ColorBy = "ParticleType"            # every particle has an own
                                               # color (Geant4 defaults)
```

Figure B.1: TOPAS example file for creating 1D and 2D depth-dose-curves by scoring dose in a cylinder water phantom divided into z-bins and in a box water phantom divided into x- and z-bins.

B.2 PYTHON Example File

```python
'''Program to read in depth-dose-curve data from a csv file and to analyze and
visualize them.'''

########################################################################
# python modules
########################################################################

from __future__ import division        # division floating point numbers
from numpy import *                     # array commands
import matplotlib.pyplot as plt         # graphics
import csv                              # reading csv-files
print __doc__                           # showing program text


########################################################################
# read in data
########################################################################

data1 = genfromtxt('/Applications/topas/Jan/RangeAnalyse/BP/BP-200-100000.csv',
                    delimiter = ',')       # topas data

z1 = 0.01*data1.T[2] *2                       # Depth in mm
binsize = max(z1)/len(z1)
z1 = z1 + binsize/2                        # values moved in bin center
D1 = data1.T[3]                           # topas dose
D1 = 100 * D1/max(D1)                      # normed to 100 %


########################################################################
# range analyze functions
########################################################################

def RangeBragg(z, E):
    """function calculates for a depth-dose-curve E(z) the range of maximum
    dose EMax and the related vector component i."""
    EMax = max(E)
    for i in range(len(E)):
        if E[i] == EMax:
            return z[i], i
```

```python
def RangeAfter(z, E, p2):
    """Function calculates for a depth-dose-curve E(z) the range corresponding
    to a dose of p2 times maximum dose of after dose maximum value. The value
    where dose is as close as possible to the given percentage value is
    calculated, and after a linear regression is started for the points next
    to the value. On this line the corresponding range is calculated again
    more exactly."""
    EMax = max(E)
    for i in range(len(E)):
        if i >= RangeBragg(z,E)[1] and E[i] <= p2*EMax:
            # arrays for linear regression
            arrE = array([E[i-1], E[i] ])
            arrz = array([z[i-1], z[i] ])
            zn = array([ arrz, ones(len(arrz))])
            w1 = linalg.lstsq(zn.T, arrE)[0]
            # linear regression with numpy
            z1 = linspace(z[i-5],z[i+5], 100)
            # arguments for regression line
            line1 = w1[0]*z1+w1[1]
            for j in range(len(line1)):
                # second more exactly range analyze on the regression line
                if line1[j] <= p2*EMax:
                    return z1[j]


#########################################################################
# parameters for 4 representative points
#########################################################################

p0 = 0.9                                     # percentages
p1 = 0.8
p2 = 0.2

RM = RangeBragg(z1, D1)[0]                    # 4 ranges
R09 = RangeAfter(z1, D1, p0)
R08 = RangeAfter(z1, D1, p1)
R02 = RangeAfter(z1, D1, p2)

DMax1 = max(D1)                              # 4 corresponding doses
D09 = p0 * DMax1
D08 = p1 * DMax1
```

```
###########################################################################
# parameters for 4 representative points
###########################################################################

p0 = 0.9                                        # percentages
p1 = 0.8
p2 = 0.2

RM = RangeBragg(z1, D1)[0]                       # 4 ranges
R09 = RangeAfter(z1, D1, p0)
R08 = RangeAfter(z1, D1, p1)
R02 = RangeAfter(z1, D1, p2)

DMax1 = max(D1)                                  # 4 corresponding doses
D09 = p0 * DMax1
D08 = p1 * DMax1
D02 = p2 * DMax1


###########################################################################
# visualization
###########################################################################

fig = plt.figure(figsize=(16, 7))               # figure and axes settings

ax1 = plt.subplot(111)
ax1.set_xlabel("Depth [mm]", fontsize=20)
ax1.set_ylabel("$D_{rel}$ [$\%$]", fontsize=20)
ax1.tick_params(axis='both', which='major', labelsize=20)
ax1.axis([0, 600, 0, 1.2 * DMax1])
grid = ax1.grid(True, color="k", linewidth=5, alpha=0.5)

# ploting depth-dose-curve and the 4 points
ax1.plot(z1, D1, 'b', marker="o", alpha=0.5, linestyle="None", \
            markersize=8, label='TOPAS data')       # data
ax1.plot(RM, DMax1, color="r", marker="o", alpha=1, markersize=10, \
            label="$R_{max}$" )
ax1.plot(R09, D09, color="r", marker="o", alpha=0.8, markersize=10, \
            label="$R_{0,9}$" )
ax1.plot(R08, D08, color="r", marker="o", alpha=0.6, markersize=10, \
            label="$R_{0,8}$" )
ax1.plot(R02, D02, color="r", marker="o", alpha=0.4, markersize=10, \
            label="$R_{0,2}$" )

# box with point parameters
textstr = '$R_{max}=%.2f [mm] \ \ D_{max}=%.2f $\n $R_{0,9}=%.2f [mm] \ \ \
D_{0,9}=%.2f $\n $R_{0,8}=%.2f [mm] \ \ D_{0,8}=%.2f $\n $R_{0,2}=%.2f [mm] \
\ \ D_{0,2}=%.2f $'%(RM, DMax1, R09, D09, R08, D08, R02, D02)
props = dict(boxstyle='round', facecolor='wheat', alpha=0.5)
ax1.text(0.01, 0.95, textstr, transform=ax1.transAxes, fontsize=23,
            verticalalignment='top', bbox=props)

# legend
legend=ax1.legend(loc='upper center')
plt.show()
```

Figure B.2: Python file to read in the csv-file 'Data-Cylinder1.csv' created by the previous TOPAS file and to visualize 1D depth-dose-curve of a 140 MeV proton beam.

List of Figures

List of Tables

C Bibliography

[1] Globocan 2012. Estimated incidence, mortality and prevalence worldwide in 2012, 2012. 1

[2] R.J. Schneider J.M. Sisterson M.S. Wagner B. Gottschalk, A.M. Koehler. Multiple Coulomb scattering of 160 MeV protons. *Nucl Inst Methods*, 1993. (document), 2.2, 2.5, 7.3

[3] Hans Bichsel. 2.18-MeV protons scattered from a 3.42-mg/cm^2 Al foil. *Physical Review Letters*, 1958. 2.6

[4] Geant4 Collaboration. *Geant4 Physics Reference Manual.* Application Developers, Geant4 9.5.0 edition, december 2011. 7.3

[5] Geant4 Collaboration. *Geant4 User's Guide for Application Developers.* Application Developers, Geant4 9.5.0 edition, december 2011. 2.7, 2.7, A.1, A.5

[6] C. Zacharatou Jarlskog and H. Paganetti. Physics settings for using the Geant4 toolkit in proton therapy. *IEEE Trans. Nucl. Sci. 55*, 2008. A.2

[7] J. Schümann B. Faddegon H. Paganetti Joseph Perl, J. Shin. Topas: An innovative proton Monte Carlo platform for research and clinical applications. *Medical Physics 39*, 39, November. (document), 2.7, 7.5

[8] Tobias Kunz. Diplomarbeit: Entwicklung einer Simulationsumgebung für das COMPASS-II-Experiment mit Geant4, November 2012. 2.7, 2.7, 2.7

[9] H.H. Andersen H. Bichsel D. Powers S.M. Seltzer M.J. Berger, M. Inokuti. ICRU 49, 1993. (document), 2.4

[10] NIST National Institute of Standards and Technology. PSTAR stopping power and range tables for protons, 2014. 4.3

[11] Harald Paganetti. *Proton Therapy Physics, Series in Medical Physics and Biomedical Engineering.* CRC Press Taylor and Francis Group, 1 edition, 2012. 1, 2.1, 2.1, 2.1, 2.1, 2.1, 2.2, 2.2, 2.3, 2.4, 2.2, 2.2, 2.7, 2.8, 2.2, 2.3, 2.3, 2.1, 2.9, 2.6, 7.5

[12] Joseph Perl. *TOPAS User Guide.* MGH (Massachusetts General Hospital), UCF (University of Calafornia and San Francisco), SLAC (National Accelerator Laberatory), Authorized TOPAS Beta Users, 1.0-b10 edition, march 2014. 2.1, 2.10, 2.11, 3.2, A.1, A.2, A.2, A.3, A.3, A.3, A.3, A.4, A.3, A.4, A.5, 7.5

[13] Ramos-Mendez. Geometrical splitting technique to improve the computational efficiency in monte carlo calculations for proton therapy. *Medical Physics 40*, 40, 2013. A.3

[14] Stephen M. Seltzer. An assessment of the role of charged secondaries from non-elastic nuclear interactions by therapy proton beams in water. *NIST technical note*, 1993. 2.3, 2.3

[15] Sander Bastiaan Uilkema. Master thesis: Proton therapy planning using the S_N method with the Fokker-Planck approximation, October 2012. 2.5, 2.5, 2.5, 2.5

[11] [12] [7]

Acknowledgements

I would like to express my gratitude to my supervisor Dr. Armin Lühr for the useful comments, remarks and engagement through the learning process of this bachelor thesis.

Besides my supervisor, I would like to thank my referees Prof. Dr. Arno Staessner and Prof. Dr. Wolfgang Enghardt for their encouragement, insightful comments, and hard questions.

Furthermore I would like to thank Jan Erik Wichmann, Dr. Chiranjib Mukherjee, Markus Firmbach, Sarah Krebs, Jonathan Brisch and again Dr. Armin Lühr for the endurance to check this thesis for style, spelling, grammar and content uncertainties.

Finally, I would like to thank my family for their continuous support during my studies and Janneke Grau for all these motivating post cards.

Erklärung

Hiermit erkläre ich, dass ich diese Arbeit im Rahmen der Betreuung am Institut für Physik ohne unzulässige Hilfe Dritter verfasst und alle Quellen als solche gekennzeichnet habe.

Jan Eulitz
Dresden, Oktober 2014